ACS OMEGA

http://pubs.acs.org/journal/acsodf

Review

Recent Progress in Aqueous Ammonium-Ion Batteries

Ying Wang* and Shelton F. Kuchena

Cite This: *ACS Omega* 2022, 7, 33732−33748

Read Online

ACCESS | Metrics & More | Article Recommendations

ABSTRACT: Batteries using a water-based electrolyte have the potential to be safer, more durable, less prone to thermal runaways, and less costly than current lithium batteries using an organic solvent. Among the possible aqueous battery options, ammonium-ion batteries (AIBs) are very appealing because the base materials are light, safe, inexpensive, and widely available. This review gives a concise and useful survey of recent progress on emerging AIBs, starting with a brief overview of AIBs, followed by cathode materials, anode materials, electrolytes, and various devices based on ammonium-ion storage. Aside from summarizing the most updated electrodes/electrolytes in AIBs, this review highlights fundamental mechanistic studies in AIBs and state-of-the art applications of ammonium-ion storage. The present work reviews various theoretical efforts and the spectrum studies that have been used to explore ionic transport kinetics, electrolyte structure, solvation behavior of ammonium ions, and the intercalation mechanism in the host structure. Furthermore, diverse applications of ammonium-ion storage apart from aqueous AIBs are discussed, including flexible AIBs, AIBs that can operate across a wide temperature range, ammonium-ion supercapacitors, and battery−supercapacitor hybrid devices. Finally, the review is concluded with perspectives of AIBs, challenges remaining in the field, and possible research directions to address these challenges to boost the performance of AIBs for real-world practical applications.

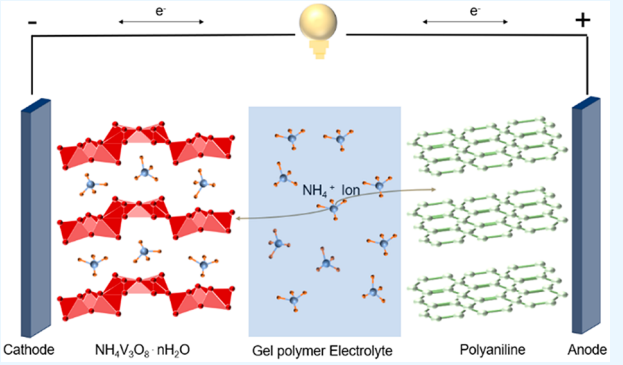

1. INTRODUCTION

One of the pressing challenges for the energy sector is to develop energy storage technologies that are safe and affordable, which are needed for a wide set of applications ranging from grid energy storage, to electric vehicles, to wearable electronics, etc. The lithium-ion battery, the most popular battery technology powering much of our digital and mobile lifestyle, has posed limitations for broader future use, mainly because of concerns raised over their cost, safety, and environmental impact. Most of these concerns come from its use of organic electrolytes that are viscous, flammable, and toxic, as well as the high price of lithium due to limited lithium sources. Hence, tremendous research efforts have been devoted to the study of aqueous electrolytes, as they are safe, convenient, inexpensive, more durable, and less prone to thermal runaways. Its higher ionic conductivity combined with simplicity of the chemistry environment may facilitate long cycle life of the battery, too.

In the case of charge carriers, multivalent metal ions (e.g., Zn^{2+}, Mg^{2+}, Ca^{2+}, Al^{3+}) have been extensively explored as alternative candidates to meet the increasing demands for energy storage and address the shortfall of lithium.[1−4] Magnesium has a low reduction potential of −2.37 V vs SHE and a high volumetric capacity of 3.833 A h/cm^3. The aluminum redox chemistry involves three-electron transfer processes, leading to an even higher volumetric capacity of 8.04 A h cm^{-3}.[5] Zinc has a high theoretical capacity of 820 mA h g^{-1} and a lower redox potential of 0.76 V vs SHE. However, problems exist, such as high electrostatic interaction between multivalent ions, corrosion in aqueous electrolytes, and dissolution of elements. For example, zinc-ion batteries have demonstrated high capacities as well as excellent rate capability and good cycling stability. Nevertheless, issues such as self-aggregation, phase change during Zn^{2+} intercalation, and heaviness of the zinc anode remain challenges for the commercialization of zinc-ion batteries.

Due to the above-mentioned reasons, research attention has been shifted toward nonmetallic charge carriers, such as protons (H^+), hydronium (H_3O^+), and ammonium (NH_4^+), which have physical characteristics that could be advantageous for any electrochemical system.[6,7] Among the three, ammonium ions as charge carriers yielding a mildly acidic electrolyte are the most appealing, whereas protons or

Received: June 30, 2022
Accepted: August 26, 2022
Published: September 13, 2022

Table 1. Summary of Various PBAs as Cathodes for Ammonium-Ion Batteries

cathode material	potential range	electrolyte	capacity (mAh g^{-1})/specific current (mA g^{-1})	ref
CuHCF	0.16−1.4 V vs SHE	0.5 M $(NH_4)_2SO_4$	55/500	17
Ni-APW	0.2−0.9 V vs Ag/AgCl	1 M $(NH_4)_2SO_4$	51.3/300	18
NiHCF	0.4−1.0 V vs SHE	0.5 M $(NH_4)_2SO_4$	38/500	17
N-CuHCF	0.5−1.0 V vs SCE	0.01 M Cu $(NO_3)_2$ + 2.0 M NH_4NO_3	53.1/1000	19
MnHCF	0−1 V vs Ag/AgCl	1 M NH_4TFSI	104/100	20
Berlin Green	−0.2−1.2 V vs Ag/AgCl	0.5 M $(NH_4)_2SO_4$	80/5000	21
$Fe_4[Fe(CN)_6]_3$	− 1 V vs Ag/AgCl	1 M $(NH_4)_2SO_4$	40/1800	22
$K_{0.9}Cu_{1.3}Fe(CN)_6$	0.4−1.4 V vs Ag/AgCl	0.5 M $(NH_4)_2SO_4$	60/50	23
NaFeIII [FeII$(CN)_6$]	0.2−0.8 V vs Ag/AgCl	1.0 M $(NH_4)_2SO_4$	60/250	24
$V_{1.5}Fe(CN)_6$	−0.4−1.2 V vs Ag/AgCl	1.0 M $(NH_4)_2SO_4$	100/2000	25
$Na_{1.45}Fe$ $[Fe(CN)_6]_{0.93}$	−0.1−0.9 V vs Ag/AgCl	1.0 M $(NH_4)_2SO_4$ + 20 mM $ZnSO_4$	75/250	26
$(NH_4)_2Cu$ [Fe$(CN)_6$]	0.2−1 V vs Ag/AgCl	1.0 M $(NH_4)_2SO_4$	77.8/150	27

hydronium ions result in a stronger acidic environment that may corrode the electrodes. In comparison with metallic charge carriers, NH_4^+ ions offer several distinct advantages as follows: (i) favorable sustainability and nontoxicity as it could be synthesized from infinite or unlimited sources (nitrogen and hydrogen in air); (ii) a lighter mass of 18 mol/g for high energy density batteries; (iii) the smallest hydration radius of 3.31 Å (despite its large ionic radius of 1.48 Å) leading to fast ion diffusion in the electrolyte; (iv) the nonmetallic interaction between NH_4^+ ion and host materials (e.g., hydrogen bond) being more flexible than the rigid metal coordination; (v) non-diffusion-controlled topochemistry between nonmetallic charge carriers and electrode framework during insertion/extraction processes leading to pseudocapacitive-dominated behavior and thus ultrafast kinetics.[8−10]

Despite the small hydration size and fast diffusion of NH_4^+ in the electrolyte, its ionic size is larger than those of most metallic carriers. Thus, it requires host materials with larger interlayer spacing or wider open structure to accommodate NH_4^+. Additionally, the sluggish redox kinetics of NH_4^+ ions limits the choice of host materials and leads to poor electrode conductivity and thus affects the battery performance due to the increased polarization of the ammonium-ion battery (AIB). The interfacial chemistry and the transport kinetics of the battery are crucial to the performance of the AIBs. Nevertheless, there is no quantitative account of the explicit role played by the electrolyte or electrode in the interfacial chemistry of ammonium-ion batteries. Finally, most ammonium-ion batteries reported in the literature deliver a very narrow voltage window of ∼1 V, leaving much space to improve. It was also discovered that the liquid-state electrolyte (1 M NH_4Cl) could dissolve some electrode material (V_2O_5/PANI composite) in ammonium-ion storage after only 400 cycles, while the device based on the gel electrolyte is stable even after 4000 cycles, indicating a possible stability issue of aqueous AIBs.[11] Thus, it can be seen that the development of AIBs is still at an early stage and hindered by the obstacles above. It would be very helpful to have a comprehensive review article thoroughly summarizing and digesting all of the information in this emerging area.

Two review articles concerning ammonium-ion batteries have appeared lately. One minireview provides comprehensive summaries of the cathodes, anodes, electrolytes, and full cells, covering structure, properties, and performances of electrode/electrolyte materials in the AIBs.[12] The other adds more details, including the working principle of AIBs and various experimental tools for characterizing morphology, structure, and composition of the battery components.[13] The study of aqueous batteries is a fast-moving field, and with publications appearing on a daily basis, it is necessary to reveal the most recent progress in AIBs with more in-depth discussions detailing the theoretical/experimental explorations of fundamental factors that are lacking in the previous review articles. Aside from summarizing the most updated electrodes and electrolytes in AIBs, this review highlights fundamental mechanistic studies in AIBs and state-of-the-art applications of ammonium-ion storage. The present work reviews various simulation efforts and spectrum studies that have been used to explore the ionic transport kinetics, electrolyte structure, solvation behavior of ammonium ions, and intercalation mechanism in the host structure. Furthermore, diverse applications of ammonium-ion storage apart from aqueous ammonium-ion batteries are provided, including flexible ammonium-ion batteries, AIBs that can operate across a wide temperature range, ammonium-ion supercapacitors, and battery−supercapacitor hybrid devices. Finally, perspectives of AIBs, challenges remaining in the field, and possible future research directions to address the challenges are discussed.

2. ELECTRODE MATERIALS FOR AMMONIUM-ION BATTERIES

2.1. Cathode Materials. The capacity of a full battery is more limited by the cathode than by the anode. Hence, it is crucial to explore high-performance cathode materials for emerging ammonium-ion batteries. The best cathode materials for batteries should exhibit good properties such as high operating voltage, large interlayer spacing, an open framework that can accommodate the large NH_4^+ ions during cycling, and a highly reversible redox reaction. The subsections below present representative cathode materials that have been developed recently for AIBs.

2.1.1. Prussian Blue Analogues. Prussian blue analogues (PBAs) are derived from Prussian blue (PB) that are ligands with strong open frameworks.[14−16] Their cubic geometry and open framework structure enable rapid ionic transport and good rate capability. During the ion insertion process, their geometry does not change much, which is impressive for long cycling. Due to their unique geometric shape and structural stability, the PBAs are good candidates for NH_4^+ ion storage. The empirical formula of PBAs is $A_xL_y[M(CN)_6]_z{\cdot}nH_2O$, where A is metal ion or NH_4^+ and L and M are transition metal ions. The PBA framework results from the transition metal ion bonded to six nitrogen and carbon atoms to form the −C≡N− bonds.

https://doi.org/10.1021/acsomega.2c04118
ACS Omega 2022, 7, 33732−33748

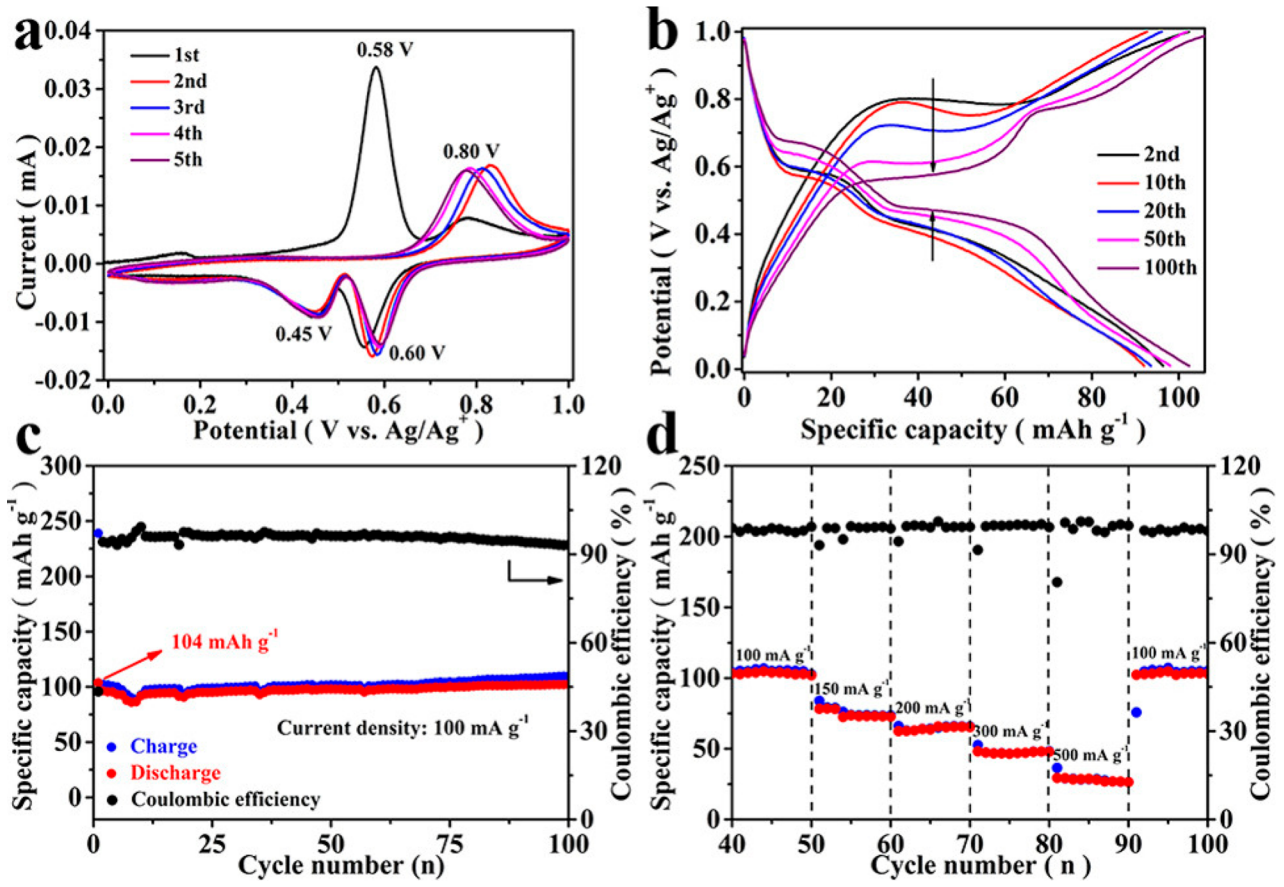

Figure 1. Electrochemical characterizations of MnHCF. (a) First five CV curves at a scan rate of 0.05 mV/s (b) Galvanic charge−discharge curves from 0 to 1.0 V at 0.1 A g^{-1}. (c) Cycling performance at 0.1 A g^{-1}. (d) Rate performance. Reproduced with permission from ref 20. Copyright 2022 Wiley.

The first work on NH_4^+ storage was performed by Wu's group using PBAs, NiHCF and CuHCF, because of their open structure and strong structural integrity.[21] In comparison with other monovalent metal ions such as Li^+, Na^+, and K^+, the NH_4^+ ion intercalation shows the highest intercalation potential of 1.0 V vs SHE and delivers a capacity of 60 mAh g^{-1}. Another important research was carried out by Ji's group in fabricating a full ammonium-ion battery using a PBA cathode and an organic anode.[27] In this work, $(NH_4)_{1.47}Ni[Fe(CN)_6]_{0.88}$ was synthesized to serve as both a cathode material and an NH_4^+ ion source, to combine with the 3,4,9,10-perylenetetracarboxylic diimide (PTCDI) anode and 1.0 M aqueous $(NH_4)_2SO_4$ electrolyte. The resulting full cell delivers a capacity of ∼50 mAh g^{-1} at a specific current of 120 mA g^{-1}, achieving a specific energy of 43 Wh kg^{-1}. To date, various PBAs have been synthesized, and their performances are summarized in Table 1.

PBA materials usually show ammonium-ion storage capacities lower than 100 mAh/g. However, a manganese-based Prussian white analogue (MnHCF) was recently obtained that delivered higher capacities for NH_4^+ ion storage.[20] Figure 1a displays the cyclic voltammetry (CV) curve of the MnHCF electrode in a potential range of 0−1 V, revealing major peaks at 0.58, 0.80, 0.60, and 0.45 V. Figure 1b reveals that the overpotential decreased as the cycling goes on, indicating MnHCF being activated as the cycling continued. The cycling performance of this electrode in Figure 1c exhibits a capacity retention of 98% from the initial capacity of 104 mAh g^{-1} at 0.1 A g^{-1}. The rate performance of MnHCF in Figure 1d displays 104, 78, 66, 48, and 30 mAh g^{-1} at specific currents of 100, 150, 200, 300, and 500 mA g^{-1}, respectively. To form a full cell, an organic electrolyte with bis(trifluoromethane)sulfonimide ammonium (NH_4TFSI) in tetraethylene glycol dimethyl ether (TEGDME) was combined with the MnHCF cathode and 3,4,9,10-perylenetetracarboxylic diimide (PTCDI) anode, delivering a capacity of 45 mAh g^{-1} at 15 mAh g^{-1}.

The (de)intercalation mechanism of NH_4^+ ions in PBAs was investigated by Shu at al. for CuHCF, with the reaction mechanism formula as follows:[22]

$$Cu_{2.95}[Fe^{III}_{0.75}Fe^{II}_{0.25}(CN)_6]_{1.69} + 2e^- + 2NH_4^+ \leftrightarrow (NH_4)_2Cu_{2.95}[Fe^{II}(CN)_6]_{1.69}$$

Additionally, spectroscopic techniques such as ex situ Fourier transform infrared (FTIR), nuclear magnetic resonance (NMR), and theoretical simulations, were used to reveal hydrogen bonds between NH_4^+ ions and N atoms in the Fe−PBA system, and it was found that they are responsible for charge transfer.[22] Such a phenomenon was not observed for metallic charge carriers in PBAs, such as Na^+ and K^+ ions. These results show that PBAs are good cathode materials for AIBs; nevertheless, there is room to improve their capacities.

2.1.2. Metallic Oxides. Transition metal oxides are commonly used as electrode materials for a variety of rechargeable batteries. Some of them with large open structure

https://doi.org/10.1021/acsomega.2c04118
ACS Omega 2022, 7, 33732−33748

Table 2. Summary of Oxide Cathode Materials for Ammonium-Ion Batteries

cathode	potential range	electrolyte	capacity (mAh g^{-1})/specific current (mA g^{-1})	ref
V_2O_5	−0.2−0.8 V vs Ag/AgCl	0.5 M $(NH_4)_2SO_4$	70/5000	28
MnO_x	0−0.8 V vs Ag/AgCl	0.5 M NH_4Ac	175/500	29
$Fe_5V_{15}O_{39}(OH)_9{\cdot}9H_2O$	−0.4−1.2 V vs Ag/AgCl	0.5 M $(NH_4)_2SO_4$	130/100	30
$NH_4V_4O_{10}$	0−1 V (full cell)	1 M $(NH_4)_2SO_4$	103/100	31
$NH_4V_3O_8$	0−1 V (full cell)	1 M $(NH_4)_2SO_4$	110/100	61
hetero-VS_2/VO_x	−0.6−0.9 V vs Ag/AgCl	5 M $(NH_4)_2SO_4$	200/100	32
PANI/$Na_{0.73}Ni[Fe(CN)_6]_{0.88}$	0−1 V vs Ag/AgCl	1 M $(NH_4)_2SO_4$	92.5/100	33

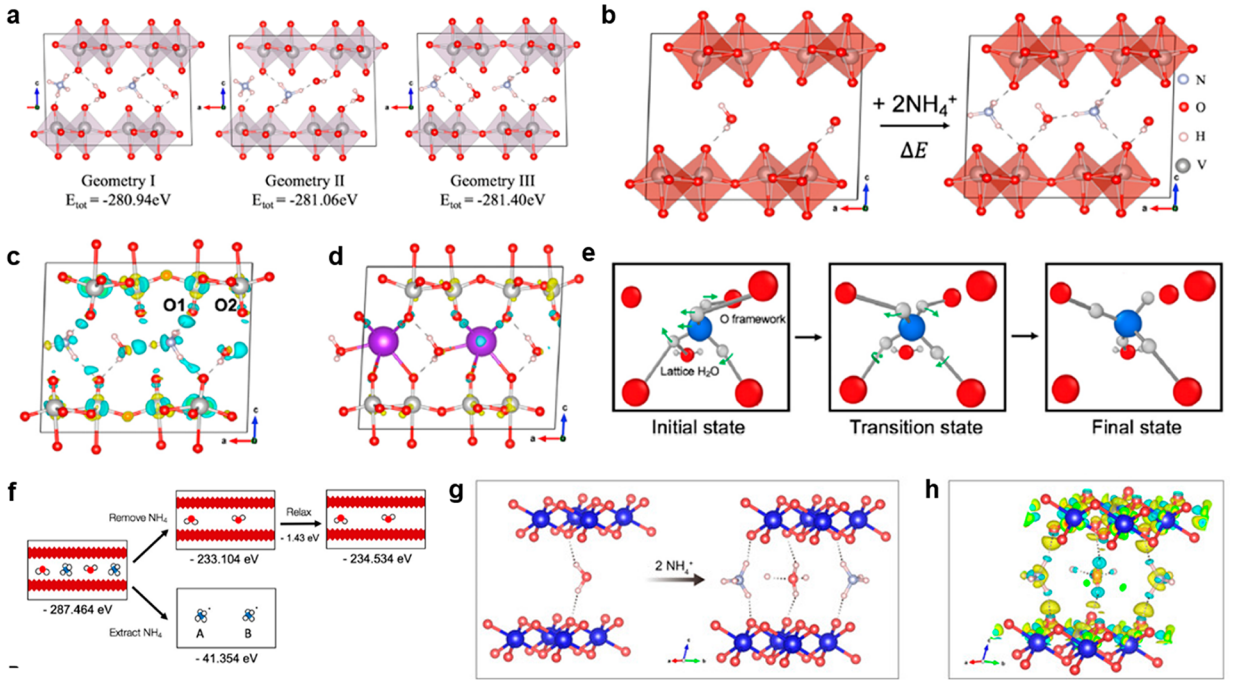

Figure 2. (a) Three geometries of the simulated $(NH_4)_{0.5}V_2O_5{\cdot}0.5H_2O$. (b) Ammonium-ion intercalation process in the V_2O_5 structure, resulting in $(NH_4)_{0.5}V_2O_5{\cdot}0.5H_2O$. (C) Charge density difference for the reduced V_2O_5 electrode in (b), charge transfer from V O═V (yellow lobes) to H··· O═V (blue cloud) oxidizing the attached V. (d) K^+ ion intercalation into the VO framework (in (b,c), the charge distribution densities are blue for electron accumulation and yellow for depletion). (e) NH_4^+ ion diffusion mechanism showing the breaking and formation of hydrogen bonds. (f) Binding energy calculation for $(NH_4)_{0.5}V_2O_5{\cdot}0.5H_2O$. Panels (e,f) are reproduced with permission from ref 28. Copyright 2019 Elsevier. (g) Ammonium-ion intercalation in MnO_2. (h) Charge density distribution on the NH_4^+ ion inside MnO_2. Panels (g,h) are reproduced with permission from ref 29. Copyright 2021 Wiley.

or wide interlayer structure, such as MoO_3, V_2O_5, FeVO, and MnO, have been investigated as cathode materials in ammonium-ion batteries. Transition metals have rich valence states that can vary, achieving a stable structure with other ions. For example, the valence state of vanadium can change from +2 to +5, implying that multielectron transfers can be utilized and high capacities can be achieved as a result. Bilayered V_2O_5 has been reported to show good NH_4^+ ion storage performance, delivering a reversible capacity of 100 m Ah g^{-1} at a specific current of 0.1 A g^{-1} and a capacity retention of 80% after 30000 cycles at 5 A g^{-1}.[28] MnO_x, another common cathode material for batteries, has been studied for NH_4^+ ion storage, exhibiting a high specific capacity of 176 mA h g^{-1} at 0.5 A g^{-1} in 0.5 M CH_3COONH_4 (NH_4Ac) electrolyte.[29] When cycled in a high-concentration electrolyte such as 8 M (NH_4Ac), the MnO_x cathode inhibits an amorphous−crystalline structural transformation which induces fast capacity fading. More recently, nanosheets of iron vanadate ($Fe_5V_{15}O_{39}(OH)_9{\cdot}9H_2O$, FeVO) have been tested for intercalating NH_4^+, K^+, and Na^+ ions, delivering a capacity of 72.5, 64.7, and 17.3 mA h g^{-1}, respectively. It is clear that FeVO as an NH_4^+ intercalation electrode material shows the best performance among the three cations because of the directional hydrogen bonding that can be formed between the host and the intercalated NH_4^+ ions.[30] Additionally, preammoniated layered vanadium-based cathodes have been proposed, such as $NH_4V_4O_{10}$, serving as both an NH_4^+ charge carrier source and a cathode in a full cell. A capacity of 100 mAh g^{-1} is discovered for $NH_4V_4O_{10}$, and the full cell with a polyaniline (PANI) anode exhibits a capacity of 80 mAh g^{-1} at 0.1 A g^{-1}.[31] It would be interesting to investigate if the NH_4^+ ions in $NH_4V_4O_{10}$ would cause structural collapse during cycling, as they act as pillars to stabilize the structure. A summary of typical metallic oxides as AIB cathodes is provided in Table 2, including the working potential range, electrolyte, and capacity.

As shown above, metallic oxides are promising host materials for ammonium-ion storage, providing decent capacities. Thus, it is important to obtain a fundamental understanding of the intercalation mechanisms of ammonium ions in various lattice frameworks to gain insights into the future design of new electrode materials for AIBs. These

https://doi.org/10.1021/acsomega.2c04118
ACS Omega 2022, 7, 33732−33748

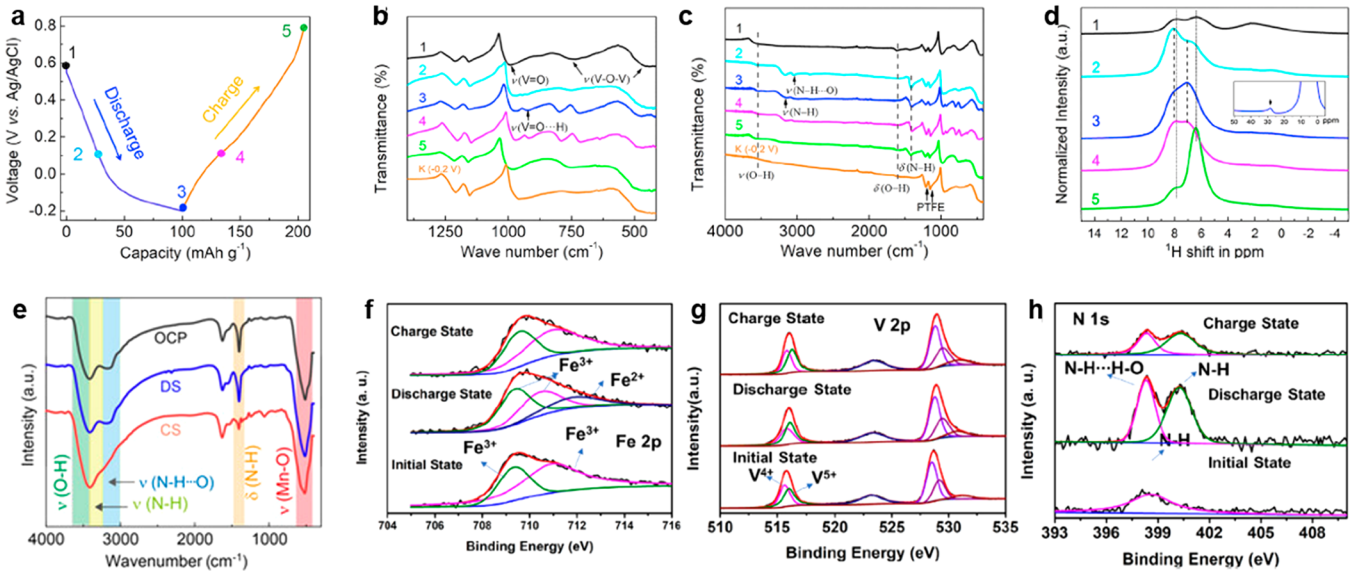

Figure 3. (a) Charge−discharge profiles of V_2O_5 in the electrolyte of 0.5 M $(NH_4)_2SO_4$ solution. (b,c) Ex situ FTIR of V_2O_5 electrode cycled with ammonium ions at different voltages, compared to the spectra of the electrode fully discharged with K^+ ion at −0.2 V. (d) NMR spectra of V_2O_5 electrode at selected voltages. Panels (a−d) are reproduced with permission from ref 28. Copyright 2019 Elsevier. (e) FTIR of MnO_x charged with NH_4^+ at different states. Panel (e) is reproduced with permission from ref 29. Copyright 2021 Wiley. XPS spectra of $Fe_5V_{15}O_{39}(OH)_9{\cdot}9H_2O$ electrode at pristine, charged, and discharged states in the AIB: (f) Fe 2p spectra, (g) V 2p spectra, (h) N 1s spectra. Panels (f−h) are reproduced with permission from ref 30. Copyright 2020 Elsevier.

mechanistic studies can be attained via molecular dynamics (MD) simulations combined with spectroscopic measurements from the macroscale to the microscale. NH_4^+ is a multipolar ion with a tetrahedral shape. During its intercalation process in the lattice of a metallic oxide, the ammonium ion rotates to move forward inside the oxide structure, with the hydrogen bonds between the ammonium ion and the host breaking and forming back and forth, thus improving the migration kinetics of ammonium ions in the oxide structure. Such a mechanism is distinctly different from those of metallic charge carriers that form rigid ionic bonds with the host material. Density functional theory (DFT) calculations have been commonly employed to examine the intercalation mechanisms in oxides, for example, ammonium-ion storage in V_2O_5.[28] In this work, the pseudocapacitive behavior of NH_4^+ ions is compared to K^+ ions, as they have similar characteristics. NH_4^+ has an ionic radius of 1.48 Å, with a coordination number (CN) of 6. The ionic radius of K^+ is 1.38 Å, and its CN is 6, too. Nevertheless, NH_4^+ storage in V_2O_5 has a different mechanism due to directional hydrogen bonding. A monkey-swinging model was proposed. In this model, the H-bond between the hydrogen in the ammonium ion and an oxygen in the VO framework breaks followed by this hydrogen bonding with another oxygen in the VO lattice, so that the ammonium ion moves like a monkey moves on branches in a tree. The NH_4^+ ion can form hydrogen bonds with the V═O structure in the VO framework, while the K^+ ion forms rigid ionic bonds with the oxide host, which leads to lower Gibbs free energy for intercalating NH_4^+ ions than accommodating K^+ ions and thus faster pseudocapacitive behavior of NH_4^+ storage in vanadium oxide.

Figure 2 illustrates the insertion mechanisms of NH_4^+ and K^+ ions in the layered V_2O_5, as understood from the DFT calculations. Figure 2a shows the possible structure of $(NH_4)_{0.5}V_2O_5{\cdot}0.5H_2O$ resulting from ammonium ions inserted in the layered V_2O_5, with geometry III having the lowest energy and thus being the most stable. When ammonium ions are intercalated into V_2O_5, they act as pillars between the adjacent bilayers of V_2O_5, forming hydrogen bonds with the oxide host to stabilize the structure after ammoniation (Figure 2b). This process causes a change in the crystallinity of the layered V_2O_5. Based on Bader charge analysis, for one NH_4^+ ion inserted, there is 0.17 electron transfer from the VO framework, resulting in the lowering of the Gibbs free energy of the electrode. $(NH_4)_{0.5}V_2O_5{\cdot}0.5H_2O$ was found to have a total energy of −287.464 eV, which is more negative than that of $K_{0.5}V_2O_5{\cdot}0.5H_2O$ (−246.245 eV), as shown in Figure 2f, indicating that the insertion of NH_4^+ ions into V_2O_5 occurs at a potential higher than that of K^+ ions. Figure 2c shows a nonbonding electron pair on O forming a dative bond with charges accumulated on O1 and O2. Figure 2d displays the movement of K^+ ions in the layered V_2O_5, while the movement of NH_4^+ ion in the oxide is presented in Figure 2e, revealing the monkey bar movement of ammonium ions breaking and forming hydrogen bonds with the host, which is different from that of metallic K^+ ions. Similar results are confirmed by another report concerning layered MnO_x, as exhibited in Figure 2g, presenting the lower energy structure composed of crystalline water and NH_4^+ ion in the layered structure of MnO_x. The Bader charge distribution in Figure 2h shows the charge transfer from the NH_4^+ ion to MnO_x. The total energy of the discharge product of the NH_4^+ ion insertion is −160.42 eV, which is lower than that of K^+ insertion (−118.97 eV), suggesting more energetically favorable insertion of the NH_4^+ ion than of K^+. These results demonstrate that NH_4^+ ions form similar hydrogen bonding with the host of MnO_x and V_2O_5, which is different from the ionic bonding formed between metallic charge carriers and the oxide electrode, providing insights into understanding the nature of chemical interactions during a nominal pseudocapacitive process.

Aside from theoretical efforts, various microscopic and spectroscopic analyses can be employed to shed light on the fundamental mechanism of ammonium-ion intercalation into

https://doi.org/10.1021/acsomega.2c04118
ACS Omega 2022, 7, 33732−33748

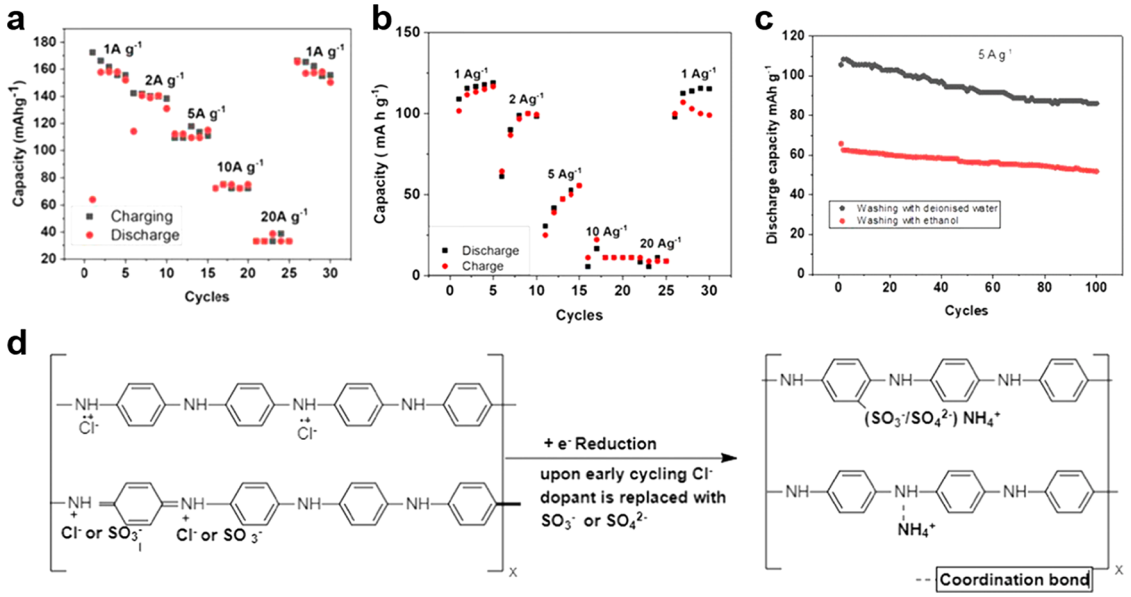

Figure 4. Rate performance of (a) ES-PANI electrode and (b) EB-PANI electrode. (c) Cycling performances of ES-PANI electrodes with different post-treatments. (d) Reaction mechanism of NH_4^+ with ES-PANI. Panels (a–d) are from ref 6. Copyright 2020 American Chemical Society.

electrode materials: scanning electron microscopy (SEM) as well as transmission electron microscopy (TEM) analyses for the changes in the morphology, energy-dispersive spectroscopy (EDS) for the elemental information, thermogravimetric analysis (TGA) for the water content in the electrode if applicable, X-ray diffraction (XRD) for the composition and crystal structure, and X-ray photon spectroscopy (XPS) for the valence state and chemical bonding environment. Bonding environment and chemical groups in the electrodes can also be examined using NMR, Raman spectroscopy, and FTIR spectroscopy. Furthermore, during charge and discharge, the cathode and the anode go through an ion transfer process, which causes changes in morphology, crystal structure, and the chemical state of the electrode material. As such, the techniques above can be combined with ex situ or in situ characterizations to reveal the changes in the morphology, crystal structure, valence state, and bonding environment of the electrodes at different charge/discharge states to understand the intercalation mechanism of charge carriers in the host material and to establish the relationships between the electrode/electrolyte structure and the electrochemical properties. For example, ex situ FTIR combined with XPS can be used to examine the H-bond formation. The interplay among NH_4^+, anions, and water can be probed with FTIR, NMR, and Raman spectroscopy. The NH_4^+ storage mechanism can thus be thoroughly examined and unveiled via intimately combining theoretical simulations, spectrum studies, and electrochemical performance evaluations.

Figure 3 presents various spectroscopic studies of three different cathode materials for ammonium-ion or potassium-ion intercalation. Figure 3a displays the charge/discharge profiles of V_2O_5 cycled in 0.5 M $(NH_4)_2SO_4$ electrolyte, with the ex situ FTIR and NMR spectra of this cathode at different charge/discharge states revealed in Figure 3b–d, respectively.[28] It can be seen that there are new peaks from V═O at ∼993 to 958 cm^{-1} corresponding to the reduction of V(V) to V(IV) in V_2O_5. There is also a new peak for the vibration of N–H in NH^+ at approximately 3050 and 3150 cm^{-1} from the cathode at different discharge states, which are attributed to the N–H forming a hydrogen bond with the VO. Figure 3d displays the NMR spectrum of the pristine cathode, showing the resonance peaks at 7.8 and 6.4 ppm corresponding to hydrogen bonds between lattice water molecules and O in the VO framework. During the ammoniation of the cathode, the NMR spectrum reveals a reduced resonance intensity, and the peaks shift from 7.2 and 6.9 ppm to 8.1 and 7.15 ppm because of the hydrogen bonding between the NH_4^+ ion and VO framework. These NMR results confirmed what is observed in the FTIR spectra. Similarly, hydrogen bonding is also observed in the MnO_x cathode intercalated with ammonium ions, as shown in Figure 3e.[29] The discharged cathode shows a new peak at 3170 cm^{-1}, which is ascribed to hydrogen bonding between N–H and O in the MnO_x framework. Apart from FTIR and NMR, XPS can also be used to probe the interactions between charge carriers and the electrode material. $Fe_5V_{15}O_{39}(OH)_9{\cdot}9H_2O$ has recently been demonstrated as an effective ammonium-ion storage material.[30] Figure 3f–h presents the XPS spectra of Fe, V, and N in the initial, charge, and discharged state of this electrode, respectively. Fe(III) can be seen to be reduced to +2 during discharge and oxidized back to +3 during charge. The same is observed for V showing +4 at the discharged state and +5 at the charged state. It is notable that the N 1s spectrum from the electrode at the discharged state exhibits two split peaks at 400.3 and 398.6 eV, corresponding to the hydrogen bonding (N–H···O) between the N–H with the host material. Hence, the formation of hydrogen bonding between ammonium ions and the oxide electrode can also be confirmed by XPS.

2.1.3. Organic Compounds. There are two major categories in which organic compounds can be classified, that is, n-type compounds and p-type compounds. An n-type organic compound undergoes reduction to form a negatively charged state (n^-) by taking an electron, and its charge is made up by a countercation. On the other hand, a p-type compound is oxidized to form a positively charged state (p^+) by losing an electron, with an anion participating in the redox reaction to compensate the positive charge.

https://doi.org/10.1021/acsomega.2c04118
ACS Omega 2022, 7, 33732–33748

Table 3. Summary of Anode Materials for Ammonium-Ion Batteries

anode material	potential range	electrolyte	capacity (mAh g^{-1})/specific current (mA g^{-1})	ref
PTCDI	−1.1−0.2 V vs Ag/AgCl	1 M $(NH_4)_2SO_4$	120/240	32
$TiO_{1.85}(OH)_{0.30}{\cdot}0.28H_2O$	−1.3 to −0.6 V vs Ag/AgCl	25 m NH_4CH_3COO	84/500	34
PNTCDA	0 to −1.0 V vs Ag/AgCl	0.5 M $(NH_4)_2SO_4$	120/1000	35
		25 M NH_4CH_3COO	160/160	
		1.0 M CH_3COONH_4	110/160	
$K_{0.38}(H_2O)_{0.82}MoS_2$	−0.4−0.8 V vs Ag/AgCl	1 M $(NH_4)_2SO_4$	50.7/500	36
alloxazine	−0.8−0.1 V vs Ag/AgCl	1 M $(NH_4)_2SO_4$	135/1000	37
h-MoO_3	0.1−1 V vs Ag/AgCl	1 M NH_4Cl	40/1800	38
PI	−0.9−0.1	1 M $(NH_4)_2SO_4$	157.3/500	39

Only a few organic compounds have been reported for application as cathode materials in AIBs. An organic polymer, poly(2,2,6,6-tetramethylpiperidinyloxy-4-yl methacrylate) (PTMA), has been investigated in 1 M $(NH_4)_2SO_4$ for ammonium-ion storage, delivering a capacity of 80 mA h g^{-1} at a specific current of 0.5 A g^{-1}.[32] To enhance the capacity for AIBs, Kuchena and Wang explored PANI.[6] In their work, polyaniline was doped with Cl^- ions to produce an emeraldine salt state (ES-PANI), while the undoped polyaniline was in the form of emeraldine base (EB-PANI). An in situ polymerization method was used to promote the oxidative polymerization on the carbon felts. The ES-PANI on the carbon felts gives a high capacity of 160 mAh g^{-1} at 1 A g^{-1}, in contrast to the capacity of 116 mAh g^{-1} from EB-PANI at the same specific current, due to the doping with Cl^- ions. This work sheds light on how doping alters the conductivity of polyaniline and improves the storage capacity of polyaniline consequently. Future work can be expected, such as exploring how doping with a different anion (e.g., SO_4^{2-}) affects the performance of PANI for application in AIBs. Figure 4a,b presents the rate performance of ES-PANI and EB-PANI electrodes, respectively. It can be seen that the capacity of ES-PANI is 160 mAh g^{-1}, and EB-PANI delivers a capacity of 116 mAh g^{-1} at 1 A/g. Figure 4c further reveals the effect of post-treatment on the electrochemical property of polyaniline. In the study, the ES-PANI electrode post-treated with DI water exhibits capacities higher that those of ethanol, possibly because washing with ethanol causes the removal of the oligomers or causes partial dedoping that results in a lower yield. In ES-PANI, the dopant Cl^- ions are in dynamic equilibrium with the polymer chain, and a solvent as a Lewis base with respect to HCl can dedope the polymer.[33] The reaction mechanism between polyaniline and ammonium ions is illustrated in Figure 4d. The NH_4^+ ions form a hydrogen bond with negative charge of n^- on the polyaniline backbone chain. Upon early cycling, there is a replacement of the Cl^- dopant with the sulfate ion from the electrolyte. The question arises whether this is a dual ion storage system where NH_4^+ ions are stored during the discharging process and SO_4^{2-} ions are stored during charging. More research is required to understand this dimension of a dual storage system in polyaniline. The storage mechanism involves NH_4^+ ions having charge transfers with the −NH− and $-NH^+$ groups in the PANI backbone, which have high electron densities, as revealed by XPS characterization of the N 1s group in which the $-NH^+-$ group and −NH− group increase in atomic percentage during the discharge process.

2.2. Anode Materials. It is more challenging to develop anode materials than cathodes due to their lower potentials. As a result, there have been fewer anode materials than cathodes reported in the literature for AIBs, as presented in Table 3. Ji's group performed pioneering research in the area of ammonium-ion batteries. In their laboratory, an amorphous titanic acid ($TiO_{1.85}(OH)_{0.30}{\cdot}0.28H_2O$) was obtained via a simple sol−gel method in 2018 when few electrode materials were explored for AIBs.[34] This electrode exhibits a capacity approximately 8 times that of the crystalline TiO_2 electrode, due to rich storage sites in the disordered structure of titanic acid, which enables strong H-bonding with intercalated ammonium ions. This electrode was found to deliver a capacity of 70 mAh g^{-1} in 25 m ammonium acetate (AmAc) and 50 mAh g^{-1} in 1 m AmAc, respectively, at 5 A g^{-1}. Though the capacity of this electrode from this early work is mediocre, the work demonstrates the benefit of using "water in salt electrolyte" (WiSE). Later, the Ji group synthesized a polyimide material as an attractive anode with much superior electrochemical properties.[35] This anode delivers a very impressive ammonium-ion storage performance in 25 m ammonium acetate, i.e., a high capacity of 160 mAh g^{-1}, an excellent rate capability of 100 C, and outstanding cycling of 30,000 cycles, confirming the capability of WiSE in capitalizing the electrode performance.

Various anode materials have been investigated for use in full ammonium-ion batteries, as summarized in Table 3. Zhang at al. presented PTCDI as the anode in an aqueous ammonium-ion dual battery, exhibiting a capacity of 120 mAh g^{-1}.[32] 1,4,5,8-Naphthalenetetracarboxylic dianhydride-derived polyimide (PNTCDA) was investigated by Qui at al. in different electrolytes, such as 0.5 M $(NH_4)_2SO_4$, 25 M NH_4CH_3COO, and 1.0 M CH_3COONH_4, delivering capacities of 120, 160, and 110 mAh g^{-1}, respectively.[35] Other anode materials, such as alloxazine, h-MoO_3, and 1,4,5,8-naphthalenetetracarboxylic dianhydride-derived polyimide (PI), were reported to be promising anode materials in AIBs, showing capacities of 135, 40, and 157 mAh g^{-1}, respectively.[37−39]

Similar to the cathodes discussed in the section above, the intercalation mechanism of ammonium ions in the anodes can be studied via a combination of theoretical and experimental efforts. For example, h-MoO_3 nanowires, synthesized via a simple hydrothermal method, were demonstrated as a promising anode material for AIBs, delivering 115 mAh g^{-1} at 1 C and 32 mAh g^{-1} at 150 C, as well as a high capacity retention of 94% over 100,000 cycles and a superior power density of 4170 W/kg at 150 C.[38] DFT calculations were further carried out to examine the interaction between the inserted NH_4^+ and this oxide host, including the lower-energy model structure, energetic interaction, and the diffusion pathway of NH_4^+. The calculated structure of the oxide was constructed by first removing the NH_4^+ and then performing structure optimization and an insertion process. A set of calculations upon the different locations of water and

https://doi.org/10.1021/acsomega.2c04118
ACS Omega 2022, 7, 33732−33748

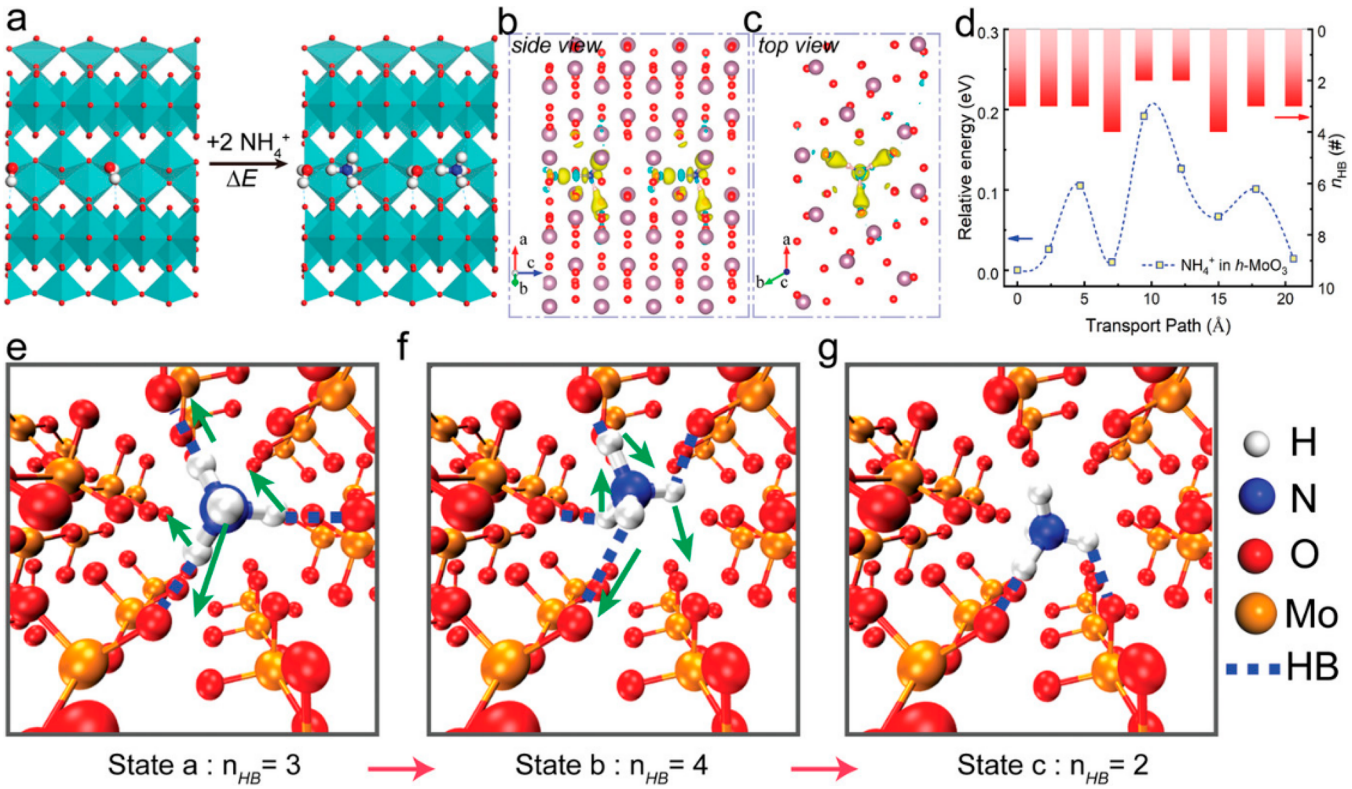

Figure 5. (a) Intercalation of NH_4^+ ions into the MoO_3 framework. (b,c) Charge distribution to realize the lowest-energy configuration. (d) Diffusion activation energy of NH_4^+ ion. (e−g) NH_4^+ diffusion process from state a to b to c. Panels (a−g) are reproduced with permission from ref 38. Copyright 2021 Wiley.

ammonium in the tunneled framework of the oxide was first conducted to determine the lower-energy model configurations, which reveal that the inserted NH_4^+ forms hydrogen bonds not only with the structural O atoms from MoO_3 but also with crystal H_2O, as displayed in Figure 5a. The variation of the interaction energy caused by insertion of one NH_4^+ in the nanotunnel and the average ion−host interaction energy for each hydrogen bonds was calculated, unveiling possible change of the host structure upon intercalation of NH_4^+. The charge density distribution shows charge being transferred from Mo═O to H···O═Mo via hydrogen bonding (Figure 5b,c). Next, the transport pathway of NH_4^+ and the corresponding relative energies along the host tunnel framework were investigated and presented in Figure 5d. Using DFT theoretical simulation, the coordination behavior of NH_4^+ ions was simulated. The adsorption energy of NH_4^+ ions was calculated to determine if the coordination configuration is thermodynamically stable or not. It was discovered that the NH_4^+ ion migrates by forming and breaking hydrogen bonds during diffusion in the oxide host (Figure 5e−g).

2.3. Other Electrode Materials. In addition to the identified AIB cathode and anode materials above, a few ammonium-ion storage materials have been developed recently, demonstrating very high capacities and other excellent performances. For instance, a solvothermal method and unique H-bond chemistry have been utilized to synthesize highly reactive covalent organic frameworks (COFs) based on quinone carbonyl oxygen and pyrazine nitrogen (QA-monomer) for application as the ammonium-ion storage material, which delivers a capacity of 220.4 mAh g^{-1} at 0.5 A/g, the highest reported so far.[40] Through theoretical simulation, it was shown that in the QA-monomer, the redox active groups are C═O and C═N, in which the carbon and pyrazine nitrogen atoms have high electron cloud densities; on the other hand, the aromatic ring does not have any charge accumulation. The gap between the carbonyl oxygen and pyrazine nitrogen becomes the electroactive site forming hydrogen bonds with the NH_4^+ ion.[46] More recently, a solution-based in situ intercalation approach has been employed to prepare nanoflower-shaped polyaniline-intercalated vanadium oxide (PVO) for increased surface area and improved ammonium-ion (de)insertion kinetics.[41] The polyaniline expands the interlayer space of the vanadium oxide structure to 13.99 Å, resulting in larger diffusion channels to accommodate ammonium ions. The transport kinetics of ammonium ions inside the electrode are thus improved by the unique π-conjugated structure of PANI, leading to high capacity, enhanced rate capability, and prolonged cycle life. Moreover, the composition of the PVO electrode can be easily optimized by tuning the ratio between PANI and vanadium oxide. The PVO with the optimized composition exhibits the highest capacity of 192.5 mAh g^{-1} at 1 A g^{-1} and 39 mAh g^{-1} at 20 A g^{-1} as well as a capacity retention of 98% over 100 cycles at both 10 and 20 A g^{-1}, demonstrating superior ammonium-ion storage, ultrafast kinetics, and promising cycling life.

Aside from the intercalation mechanism of charge carriers inside an electrode, the solvation behavior of charge carriers in the electrolyte would also impact the electrochemical performance of a battery through two aspects, i.e., affecting the ionic transport kinetics and the thermodynamic desolvation process in the electrolyte. The solvation behavior influences the formation and structure of the solid electrolyte interface (SEI) which can stabilize the electrode. Moreover, the solvation

https://doi.org/10.1021/acsomega.2c04118
ACS Omega 2022, 7, 33732−33748

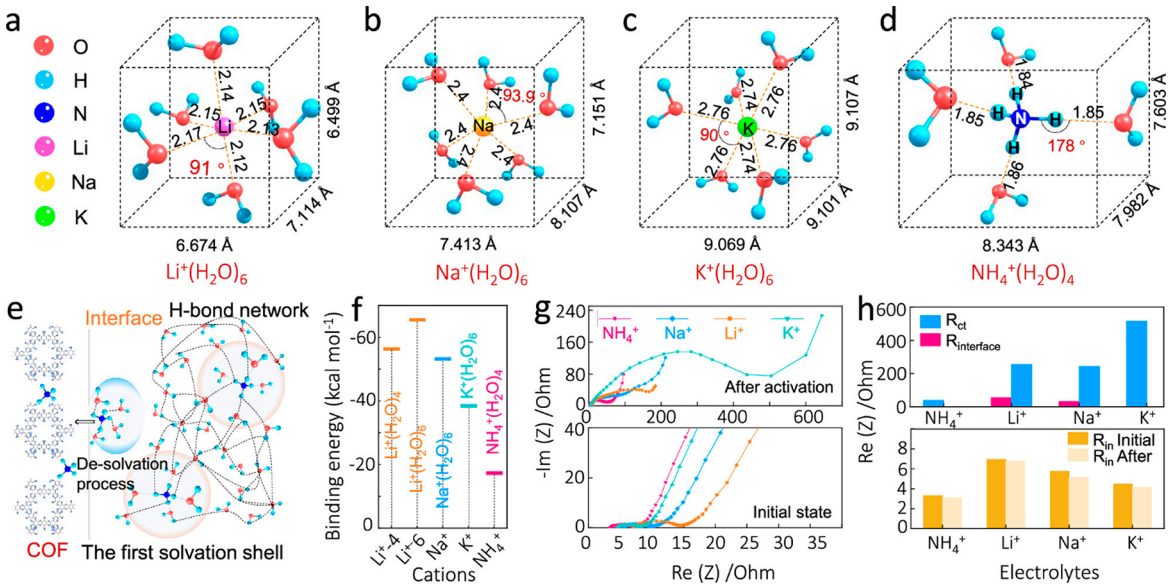

Figure 6. Solvation behaviors of Li^+, Na^+, K^+, and NH_4^+ ions. Solvation structure coordinated to six water molecules for (a) Li^+, (b) Na^+, (c) K^+ ions. (d) Four-water-molecule solvation structure of NH_4^+ ion. (e) Schematic showing the solvation behavior of NH_4^+ ion in the electrolyte. (f) Desolvation energy barriers for Li^+, Na^+, K^+, and NH_4^+ ions. (g) Nyquist plot of QA-COF in the four different electrolytes before and after electrochemical activation. (h) Impedances corresponding to the plots in (g). Panels (a–g) are reproduced from ref 46. Copyright 2021 American Chemical Society.

behavior can change the ionic conductivity, electrochemical stability window, and viscosity of the electrolytes. It also affects other physical properties of an electrolyte such as flammability, resisting overcharging, and ionic mobility at low temperatures, which would impact practical applications of the batteries. Aside from understanding the SEI effect, the comprehensive studies of the solvation structure and interfacial model (de)solvation process can guide the functional electrolyte design more effectively to improve the performance of ammonium-ion batteries, particularly with respect to high voltage, fast charge, and operation over an extended temperature range.[42−45] Spectroscopic analysis and theoretical simulations have been integrated to explore the intercalation mechanism of ammonium ions in the COFs above, confirming hydrogen bonds between NH_4^+ ion and the COFs. Additionally, the solvation behaviors of Li^+, Na^+, K^+, and NH_4^+ ions were explored and compared, as displayed in Figure 6a−d, respectively. Gaussian simulations were performed to illustrate the solvation structure of NH_4^+ in the electrolyte (Figure 6e). Compared to the bonds between metallic ions and water, the NH_4^+ ion forms a hydrogen bond with water molecules, i.e., H-bond between nitrogen atom and oxygen atom (N−H···O). As such, a stable four-coordination structure is formed in the first solvation shell as no more than four water molecules are required. Modeling is conducted to validate this speculation. Then excess water molecules spontaneously occupy the second solvation shell as a result of forming the H-bond network. The powerful H-bond network among different NH_4^+ ions and water molecules facilitates the migration of cations in the bulk electrolyte, which is verified by electrochemical impedance analysis. Though NH_4^+ ions may show a large solvation volume, they exhibit a loose solvation structure. During the desolvation process, cations that are solvated have to release attached water molecules before entering and interacting with the lattice of electrode materials, which is a nonspontaneous process. This process requires an additional amount of energy in order to overcome the binding energy between the water molecules and cations. Therefore, first solvation shell being loose would accelerate the desolvation process, due to low energy required for desolvation, as revealed by the equation below.

$$E_{\text{binding}} = E_{\text{complex}} - E_{\text{cation}} - E_{\text{water}}$$

The less negative binding energy represents a lower desolvation energy barrier, which would give the NH_4^+ sufficient free energy to accept electrons from the electrode, thereby attaining a higher redox potential. Figure 6f presents and compares the desolvation energy barrier for the four different cations. $NH_4^+(H_2O)_4$ shows the highest binding energy among the four cations and thus has the lowest desolvation energy barrier, thereby allowing the NH_4^+ sufficient free energy to accept electrons from the COF electrode and resulting in a higher redox potential. Furthermore, impedance measurements were carried out on the initial state (without electrochemical cycling) and activated state (after cycling) of the AIB to examine the internal resistance of the electrolyte (Figure 6g,h). The robust H-bond network in the NH_4^+ ion electrolytes would engender the fast diffusion of NH_4^+ along the network, successively enhancing the rate performance. On the other hand, the low desolvation energy barrier and flexible nonmetallic coordination bond would yield small charge transfer resistance from the activated state of the AIB.

3. ELECTROLYTES FOR AMMONIUM-ION BATTERIES

3.1. Traditional Diluted Electrolytes. The one molarity (M) legacy of electrolytes has been historically built on the fundamental fact that the optimum ion transport is of primary importance. The 1 M salt concentration provides a balance between the ionic carrier number that is proportional to salt dissolution and dissociation. Notably, the ionic mobility which is due to the viscosity of the electrolyte is balanced perfectly at the 1 M concentration. Therefore, conventional electrolytes

https://doi.org/10.1021/acsomega.2c04118
ACS Omega 2022, 7, 33732−33748

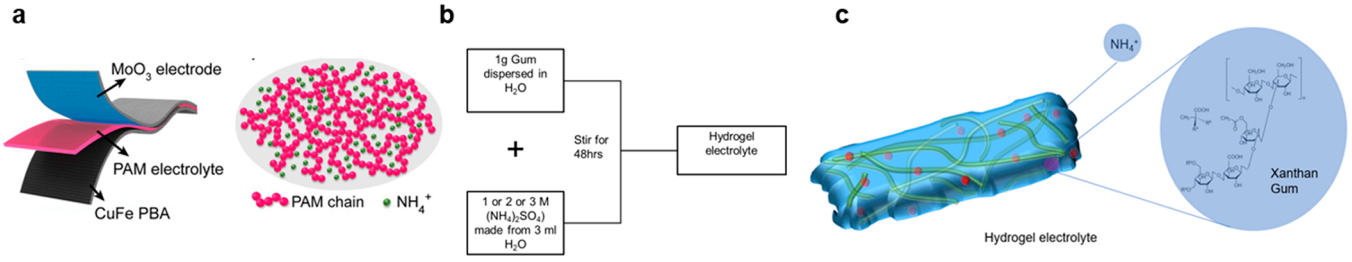

Figure 7. Schematics showing the (a) structure of the flexible battery and the PAM electrolyte. Reproduced with permission from ref 38. Copyright 2021 Wiley. Schematics showing the (b) synthesis of the hydrogel electrolyte using xanthan gum and (c) structure of the hydrogel electrolyte using xanthan gum. Panels (b,c) are reproduced with permission from ref 61. Copyright 2021 Wiley.

such as $(NH_4)_2SO_4$, NH_4Cl, NH_4NO_3, or NH_4Ac in aqueous solution have been employed in NH_4^+ storage at lower salt concentrations ranging from 0.5 to 2 M.

The traditional electrolytes are safe, convenient, easy to prepare, and lead to AIBs with decent performances. However, in a diluted salt solution, water molecules would dissociate at higher potentials to produce hydrogen and oxygen, limiting the electrochemical stability window to 1.23 V and causing undesirable side reactions that arise aside from exhaustion of water. The AIBs composed of conventional diluted electrolytes typically have a potential window of ∼1 V. These issues apparently affect the power and energy densities of ammonium-ion batteries. On another note, though a stable SEI layer can be formed from nonaqueous electrolyte, allowing electrodes to operate far beyond the thermodynamic stability limits of the electrolyte components and thus leading to a wide potential window, no stable SEI can be formed from aqueous electrolytes usually, as byproducts from water cannot be deposited in a dense solid form, which further restricts the potential window. Additionally, a diluted aqueous electrolyte can corrode the oxide electrode due to its acidity and thus impair the stability of the battery.[47] Moreover, diluted aqueous electrolyte would freeze at subzero temperatures, which hinders the adoption of ammonium-ion batteries in frigid environments. Therefore, it is imperative to modify these electrolytes or develop new electrolytes to alleviate these issues and improve the performances of AIBs for practical applications in diverse environments.

3.2. Water in Salt Electrolytes. To remedy the issues summarized in the subsection above, great strides were made in identifying the WiSE with the most promise for enhanced performance while retaining safety, by dissolving ultra-high-concentration salts in water.[48,49] In such an electrolyte, few free water molecules are available and the activity of water is suppressed. Therefore, it can restrict side reactions, such as dendrite formation, active material dissolution, and replenishing of water because pH increases with the salt concentration and thus hydrolysis is reduced. The utilization of WiSE also introduces new unprecedented interfacial chemistry that can expand the potential window and benefit the performance of the battery. For instance, an aqueous lithium-ion battery based on the WiSE was reported to achieve a wide voltage of ∼3 V, ascribed to the increased onset potential of oxygen evolution and the formation of a stable SEI layer resulting from the reduction of complex anions.[50] As such, WiSE engenders the development of new electrode materials that were previously deemed unusable in diluted aqueous electrolytes. Furthermore, WiSE would have a significantly depressed freezing point compared to water because salt molecules block water molecules from packing together when the temperature decreases, allowing AIBs to be used in cold environments.

Though WiSE has been studied in metal-ion batteries,[50−52] its utilization in ammonium-ion batteries is still in the infancy stage. The Ji group presented a much wider potential window of 2.95 V from the ammonium-ion insertion behavior of an organic electrode (PNTCDA) in 25 m ammonium acetate.[53] The other paper reported a full AIB with 19 M (M: mol/kg) ammonium acetate electrolyte delivering promising capacities from −40 to 80 °C, but no cycling data were presented and crucial information like its cycling life/stability remains unclear.[54]

At higher salt concentrations in an aqueous solution, the charge carriers become aggregated with fewer water molecules tightly bound, leading to a host of new properties including thermal, mechanical, electrochemical, and interphasial characteristics. As such, WiSEs open up a brand new horizon and bring a unique opportunity to resolve the many challenges presented by next-generation battery technology. However, understanding the new unprecedented electrochemistries, interfacial chemistries, and transport kinetics introduced by the utilization of these electrolytes in the AIBs is far from sufficient, which motivates researchers worldwide to work in this area in an effort to elucidate these fundamental aspects.

3.3. Hydrogel Electrolytes. Despite the advantages offered by WiSE, the ultrahigh salt loading in WiSE drives up the cost of the electrolyte for large-scale production, and some parasitic side reactions still exist. Additionally, the compromises in conductivity and viscosity coupled with the inevitable liquid leakage likely restrict the rate performance and safety of the battery. One approach to address the challenges associated with WiSE is to prepare a concentrated hydrogel electrolyte that can serve as a separator, providing the battery with better safety, stability, and portability. The amount of salts needed will be reduced because of the polymer bonded with water to form a network. Meanwhile, solid-state rechargeable batteries promise high energy, low cost, and improved safety. Hence, they are considered as the next-generation battery technology for electric vehicles and expected to meet other critical needs for more compact and higher-capacity energy storage devices. Additionally, flexible batteries, designed to be conformal, lightweight, and can be rolled without any loss of energy, are imperative for powering wearable electronics, smart packaging, and medical devices, etc. To develop quasi-solid-state ammonium-ion batteries, a hydrogel electrolyte provides a good matrix for ions.

A hydrogel is a cross-linked hydrophilic polymer storing high volume ratio of water within the polymer matrix. Various polymers with hydrophilic chains, e.g., xanthan gum, polyacrylamide, or poly(vinyl alcohol), can be used to obtain

https://doi.org/10.1021/acsomega.2c04118
ACS Omega 2022, 7, 33732−33748

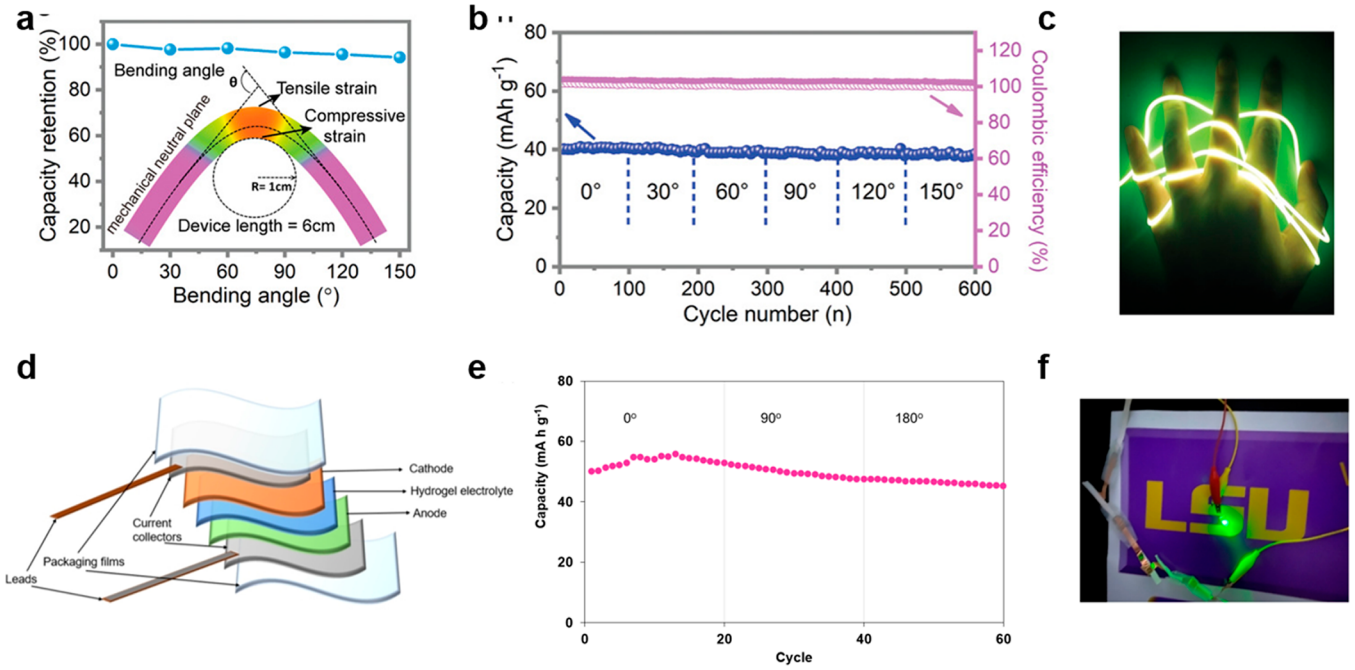

Figure 8. (a) Schematic showing the MoO_3/PBA flexible battery. (b) Cyclic performance of the MoO_3/PBA battery bent by different angles at 1 A g^{-1}. (c) Photo showing the flexible MoO_3/PBA battery lighting up a flexible luminescence fiber. Panels (a−c) are reproduced with permission from ref 38. Copyright 2021 Wiley. Photographc courtesy of Shimou Chen at al. Copyright 2022. (d) Schematic showing the structure of the flexible NH_4^+ ion battery composed of $NH_4V_3O_8$ cathode and PANI anode. (e) Cycling performance of the battery bent by different angles at a specific current of 0.1 A/g. (f) Photo showing the flexible battery lighting up LED light bulbs. Panels (d,e) are reproduced with permission from ref 61. Copyright 2021 Wiley.

hydrogels.[55,56] For instance, being natural and biodegradable makes xanthan gum an excellent choice. Its structure is composed of hydroxyl groups that can retain a great number of water molecules and long polymer chains which strengthen the coordination with water molecules.[57] Notably, xanthan gum has a high tolerance of salts, as a result of its complex exopolysaccharide structure with an α,β-1,4-linked glucan backbone and trisaccharide side chains attached to the alternating D-glucosyl residues.[58] Two methods are commonly used for preparing a hydrogel electrolyte: (i) hydrogel prepared first by mixing water and polymer, followed by soaking it in a concentrated solution of ammonium salt, and (ii) concentrated hydrogel prepared directly by mixing water, salt, and polymer. It is noted that different synthesis procedures could result in hydrogels with different mechanical properties.[59]

Though hydrogel electrolytes have been commonly adopted in metal-ion batteries, there are only two articles reporting their use in ammonium-ion batteries to date. In one report, a flexible ammonium-ion battery was demonstrated utilizing a quasi-solid-state electrolyte made from polyacrylamide (PAM) with a slat concentration of 1 M NH_4Cl solution, as displayed in Figure 7a, which had an ionic conductivity of 8.7×10^{-3} S cm^{-1} and a tensile strength of 5.84 MPa.[60] In the other report, Kuchena and Wang presented a fully flexible AIB using a concentrated hydrogel electrolyte sandwiched between an ammonium vanadate cathode and a polyaniline anode.[61] The concentrated hydrogel electrolyte was synthesized by simply mixing $(NH_4)_2SO_4$, xanthan gum, and water, as shown in Figure 7b,c. By varying the amount of salt in the electrolyte (prepared using 1, 2, or 3 m solution), it was found that the battery composed of the gel electrolyte prepared from the 3 m salt solution delivers the best initial capacity of 55 mA g^{-1} as well as good cyclability over 250 cycles at 0.1 A g^{-1}, as this electrolyte has the highest ionic conductivity of 6.1×10^{-3} S cm^{-1} and the largest tensile strength of 4.36 kPa among the three. In both of these works, the AIBs based on the hydrogel electrolytes were tested over a narrow potential window of about 1 V or slightly over 1 V. In principle, a concentrated hydrogel electrolyte can broaden the electrochemical stability window of AIBs ascribed to the reasons discussed in the section above. Nevertheless, a narrow potential window is reported, possibly because of the slower kinetics in the hydrogel electrolyte compared to that in liquid-state WiSE. Future work is needed for this emerging area to capitalize on all of the merits of concentrated hydrogel electrolytes to expand the potential window of AIBs.

In a hydrogel electrolyte, the ionic transport cannot take place without the cooperative movement of polymeric segments and solvated ions. Therefore, gel electrolytes have ionic conductivities lower than those of liquid ones, due to the lower fluidity and the inevitable interaction between the charge carriers and functional groups in the gel. Hence, flexible AIBs based on gel electrolytes deliver capacities relatively lower than those based on liquid-state WiSEs. However, the work demonstrates that the salt content in the hydrogel electrolyte can be increased and optimized to maximize the ionic conductivity of the electrolyte and electrochemical performance of the battery, though more screening of electrode materials and variations of the electrolyte compositions needs to be conducted to improve the performance of the AIBs for practical applications.

https://doi.org/10.1021/acsomega.2c04118
ACS Omega 2022, 7, 33732−33748

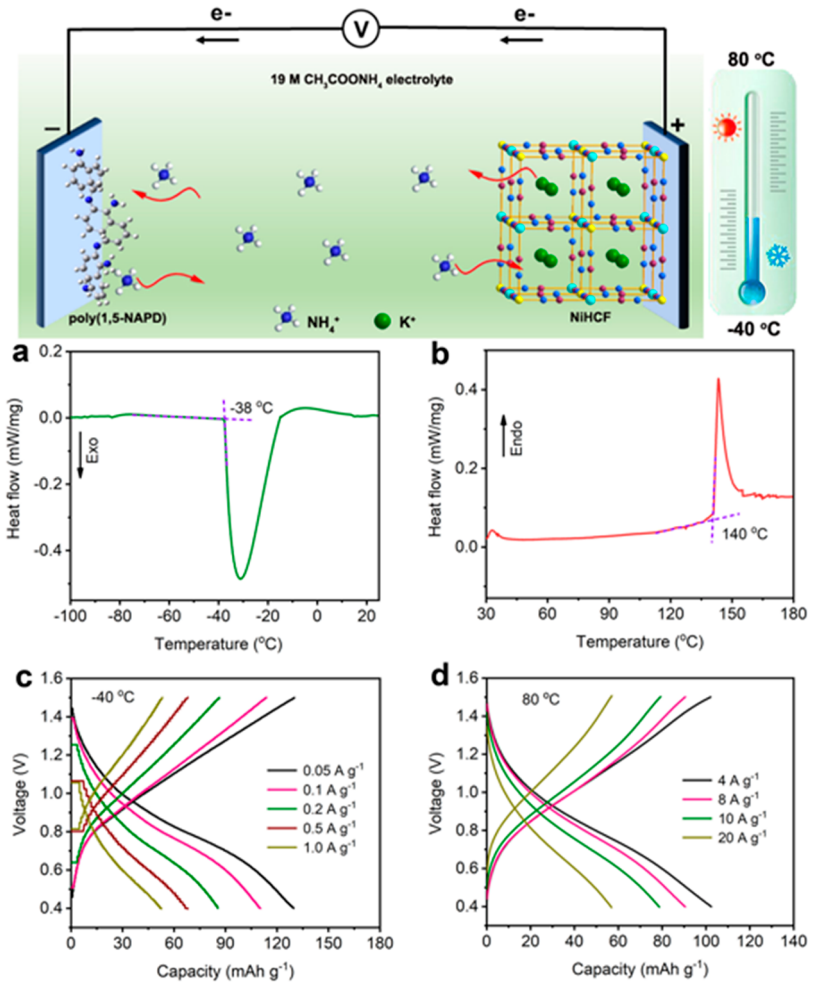

Figure 9. DSC results of the 19 M NH_4Ac electrolyte when (a) cooled to −140 °C and (b) heated to 200 °C. Charge/discharge curves of the NiHCF@CNTs//poly(1,5-NAPD) full NH_4^+ ion battery at different specific currents at (c) −40 °C and (d) 80 °C. Panels (a−d) are reproduced with permission from ref 54. Copyright 2021 Elsevier.

4. DIVERSE APPLICATIONS OF AMMONIUM-ION STORAGE

4.1. Flexible Ammonium-Ion Batteries. The rapidly increasing demands for wearable electronic devices require realization of robust flexible energy storage devices with superior electrochemical performance.[62,63] With the advancement of technology, portable electronics have become smaller and smaller with high processing speed.[64] This has sparked intense interests in developing flexible batteries to realize maximum potential of the wearable electronics.[65] It is noted that safety needs to be seriously considered in flexible batteries while they maintain high energy storage capabilities because these electronics may undergo continuous mechanical force or damage such as being struck or bent and be directly in contact with the human body.[66] Flexible ammonium-ion batteries would be very promising to power wearable devices due to their light weight and high safety, and some preliminary work has been published, one based on liquid electrolyte, one on a hydrogel electrolyte, and another on the optimized concentrated hydrogel electrolyte.

The first flexible AIB was developed in a fiber shape, with $NH_4V_4O_{10}$ coated on carbon felts as the cathode, polyaniline coated on carbon felts as the anode, and 1 M ammonium sulfate solution as the electrolyte. This flexible full cell delivers a high capacity up to 167 mAh g^{-1} at a specific current of 0.1 A g^{-1} and 54 mAh g^{-1} at 1 A g^{-1}, as well as excellent rate performance and long cycling life while under mechanical deformations. Nevertheless, it is noted the diluted aqueous electrolyte may have potential leakage issues. As such, a flexible AIB was reported using the PBA cathode, the MoO_3 anode, and the PAM hydrogel electrolyte synthesized from 1 M NH_4Cl solution, as shown in Figure 8a. This battery can be bent from 0 to 150° while retaining 90.3% capacity after 600 cycles at 1 A g^{-1}, due to the mechanical strength/stability of the PAM electrolyte (Figure 8b) and is shown to lighten up a flexible luminescent fiber (Figure 8c). Additionally, Kuchena and Wang assembled a flexible AIB using an optimized concentrated hydrogel electrolyte that was prepared from concentrated ammonium sulfate solution and xanthan gum (Figure 8d). The battery was bent at 0, 90, and 180° while undergoing electrochemical cycling, revealing a very good capacity retention of 98% and thus demonstrating excellent mechanical robustness and flexibility (Figure 8e). Figure 8f shows five connected AIBs lighting an LED light bulb, proving their potential for practical applications.

4.2. Ammonium-Ion Batteries Operating Across an Extended Temperature Range. As mentioned in section 3.2 above, significant ion pairing and aggregation occur when the salt concentration increases in an aqueous solution, while water molecules are largely bound to the cations, leading to an

https://doi.org/10.1021/acsomega.2c04118
ACS Omega 2022, 7, 33732−33748

entirely new structure at both molecular and long-range scales that affects the transport, thermal, mechanical, interfacial, and interphasial properties of the aqueous electrolyte. For instance, fewer free water molecules exist, and their mobility is decreased in a concentrated electrolyte, leading to a depressed freezing point and an increased boiling point. As such, concentrated electrolyte can be utilized to prepare ammonium-ion batteries that can operate over a wide temperature range for applications in frigid environments such as in space systems or underwater vehicles.

Though there have been several reports regarding ammonium-ion batteries based on concentrated electrolytes, there is only one article reporting some preliminary results regarding their performances at extreme temperatures. In this work, 19 M ammonium acetate solution is used as the electrolyte to combine with a Prussian blue cathode and a poly(1,5-naphthalenediamine) anode, forming an ammonium-ion battery that can work across an extended temperature range from −40 to 80 °C.[54] Figure 9a,b displays the DSC (differential scanning calorimetry) results of the 19 M NH_4Ac electrolyte down to −140 °C and heated to 200 °C, respectively, showing this electrolyte has a freezing point of −38 °C and a boiling point of 140 °C, much lower than that of pure water. For comparison purposes, 1 M NH_4Ac electrolyte was also measured with DSC, and its freezing point was found to be −30 °C. Therefore, the AIB consisting of the 19 M NH_4Ac electrolyte can function at subzero temperatures without rendering charge carriers immobile and work at elevated temperature without the electrolyte solvent evaporating. Figure 9c,d presents the charge/discharge curves of the battery at different specific currents at −40 and 80 °C, respectively. It can be seen that the battery exhibits a capacity of 130 mAh g^{-1} at 0.05 A/g at −40 °C, and a capacity of 102 mAh g^{-1} at 4 A g^{-1} is revealed for the battery at 80 °C. These results confirm the successful application of NH_4^+ redox chemistry over a wide temperature range and demonstrate the potential of the ammonium-ion batteries for applications in harsh environments. Additionally, this battery shows an energy density of 31.8 Wh kg^{-1} as well as excellent rate performance and cycling stability over 500 cycles at room temperature. Nevertheless, no cycling data of the battery were presented at subzero or elevated temperatures, indicating more work needs to be performed to fully test the battery at extreme temperatures, and possible improvements of the battery are needed for real-world applications.

4.3. Other Electrochemical Energy Storage Devices Based on Ammonium Ions. Despite the obvious merits of ammonium-ion batteries, they are relatively new, and several challenges exist such as the low operation voltage of ∼1 V, leading to low energy density. One strategy to alleviate this issue is to utilize concentrated electrolytes as discussed above. The other strategy is to fabricate new energy storage devices involving ammonium-ion storage for broader voltage and enhanced performance. One such device is the ammonium dual ion battery (ADIB). A dual ion battery (DIB) works in the way that cations are inserted into the anode together with anions intercalated in the cathode. With both cations and anions serving as charge carriers, a higher cell voltage is yielded. There are a few reports regarding the novel ADIBs to date. A green, metal-free, purely organic ADIB was assembled using p-type polyimide as the cathode, n-type polyimide as the anode, and 1 M ammonium sulfate solution as the electrolyte.[67] This ADIB exhibits a working voltage of 1.9 V that is wider than typical aqueous AIBs with a capacity retention of 86.4% after 10000 cycles at 5 A g^{-1}, in addition to a high energy density of 51.3 Wh/kg and a power density of 15.8 kW/kg.

To improve the feasibility of current AIBs for real-life applications, another method is to combine them with traditional metal-ion batteries such as zinc ion to form an ammonium−zinc hybrid battery. Recently, such a hybrid battery was fabricated using sodium iron hexacyanoferrate nanocubes as the cathode, low-cost zinc as the anode, and mixed 1 M $(NH_4)_2SO_4$ and 20 mM $ZnSO_4$ as the electrolyte.[68] This battery delivers an operating voltage of 1.3 V and a high energy density of 81.7 Wh kg^{-1}, exceeding the performances of typical AIBs and many hybrid batteries.

In addition to batteries, ammonium ions have been adopted to fabricate supercapacitors or battery−supercapacitor hybrid (BSH) devices. Supercapacitors are energy storage devices that deliver more charges faster than a battery but have inferior energy density. They can supply hundred times in terms of power per volume but cannot store as many charges per volume as batteries do.[69] Hence, supercapacitors find applications where power bursts are necessary, while high charge energy storage is not required.[70]

An ammonium vanadium oxide (NVO) framework was presented to deliver 71% capacitance retention over 14,000 cycles and a high specific capacitance of 339 F g^{-1} (610 C g^{-1}, 169 mAh g^{-1}) in NH_4Cl/PVA (poly(vinyl alcohol)) gel electrolyte in a three-electrode cell configuration, which is much higher than the specific capacitance of 268 F g^{-1} in NH_4Cl electrolyte.[71] A flexible quasi-solid-state hybrid supercapacitor was then assembled using the NVO and active carbon as electrodes with the NH_4Cl/PVA gel electrolyte, exhibiting high performance, too. In another report, a binder-free electrode, the polymer-intercalated vanadium oxide hydrate coated on active carbon cloth, was found to deliver a superior capacitance of 511 F/g at 0.5 A g^{-1} with the NH_4Cl/PVA gel electrolyte and 72% capacity retention over 10,000 cycles.[72] The polymer is poly(3,4-ethylenedioxythiophene)/poly(styrenesulfonate) (PEDOT/PSS) and expands the interlayer space in the VOH structure, leading to fast ion transport in the electrode and consequent high capacitance. A flexible quasi-solid-state supercapacitor was also fabricated using this electrode, showing an areal capacitance of 411 mF/cm^2 and an energy density of 3.2 Wh/m^2 at 1 mA/cm^2. In a similar work, polyaniline was intercalated in hydrated vanadium oxide (HVO) to expand the interlayer space of HVO from 11.0 to 13.9 Å for improved kinetics and stabilized structure during the ammonium-ion insertion.[73] The resulted PVO (polyaniline-intercalated vanadium oxide) electrode delivers 351 F g^{-1} at 1 A g^{-1}, much higher than 156 F g^{-1} from the HVO electrode. A flexible quasi-solid-state hybrid supercapacitor was then assembled using the NH_4Cl/PVA gel electrolyte sandwiched between the PVO cathode and the active carbon anode, exhibiting excellent performance and good mechanical durability.

Aside from ammonium-ion supercapacitors or hybrid supercapacitors composed of vanadium-based electrodes, research efforts have been made to achieve aqueous all-organic BSH devices that are appealing compared to traditional metal-ion batteries or supercapacitors, due to their easy fabrication, low cost, processing flexibility, and recyclability. For instance, 30 m ammonium acetate is used as electrolyte to combine with a PDI-Dh anode composed of perylenetetracarboxy diimide

https://doi.org/10.1021/acsomega.2c04118
ACS Omega 2022, 7, 33732−33748

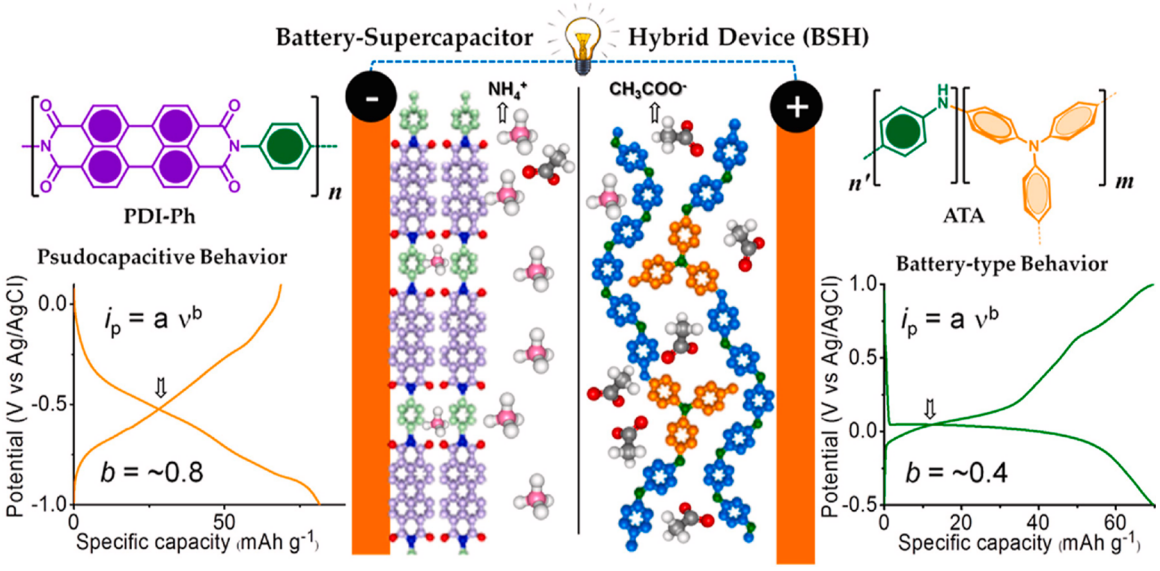

Figure 10. Schematic showing the all-organic battery−supercapacitor hybrid device, as well as capacity results of the PDI-Ph anode with pseudocapacitive behavior and the ATA cathode with the battery-type behavior. Reproduced with permission from ref 74. Copyright 2021 Elsevier.

core and an ATA cathode comprising mixed aromatic amine groups, forming an all-organic metal-free BSH device for the first time, as illustrated in Figure 10. It was discovered that the ATA cathode exhibits battery-type behavior with acetate ions in electrolyte interacting with nitrogen atoms in the ATA cathode, while the PDI-Ph anode shows pseudocapacitive behavior by intercalating ammonium ions from the electrolyte. This device reveals a wider voltage window of 2.1 V, a capacity of 42 mAh g^{-1} at 0.2 A g^{-1}, a capacity retention of 63% after 5000 cycles, a maximum energy density of 16.5 Wh kg^{-1}, and a power density of 719 Wh kg^{-1}.[74] It can be seen that the electrochemical performance of this metal-free BSH device is still very inferior to those of the vanadium-based supercapacitors above, indicating further research is needed to enhance the organic BSH devices for practical applications.

5. FUTURE OUTLOOK AND CONCLUSION

This review clearly shows that aqueous ammonium-ion batteries have tremendous potential for a wide variety of applications from stationary energy storage to powering wearable electronics, owing to their intrinsic safety, low cost, light weight, and decent performance. The realization of high-performance ammonium-ion batteries has benefitted from the developments of traditional nanostructured electrode materials, ranging from metal complexes (PBAs), metal oxides, polymers, to composites. These materials can be easily prepared via solution processing methods that have great potential for cost-effective large-scale productions. The performances of the AIBs can also be boosted using unconventional concentrated electrolytes, which would expand the potential window, allow electrode materials that are used to be unstable with diluted electrolytes, and unlock new opportunities such as freeze-tolerance properties, enabling aqueous batteries with capacities working in frigid environments. It is noted that the solvation behavior and the intercalation mechanism of ammonium ions are fundamentally different from those of metallic charge carriers in aqueous batteries, which may provide a unique opportunity to resolve the many challenges presented by next-generation battery technology. Compared to the rather rigid ionic bonds formed between metallic ions and the electrode, ammonium ions form hydrogen bonding with the host, which is more flexible and would break and form back and forth during the NH_4^+ intercalation process in the electrode, as confirmed by both spectroscopic analysis and theoretical investigations.

Despite the technological importance of aqueous ammonium-ion batteries, there is much room for improving, in order to fully capitalize the merits of the batteries and maximize the performance in all aspects. The capacities of ammonium-ion batteries are still lower than those of aqueous metal-ion batteries, possibly due to the larger ionic size of ammonium ions and consequent restricted electrode material choices as well as sluggish diffusion kinetics in the electrode. Most of the reported AIBs still deliver a very narrow voltage window of ∼1 V. In addition, most of the existent experimental characterizations of ammonium-ion batteries have focused on ex situ tests or post mortem examinations at the macroscale, which do not provide a comprehensive understanding of the underlying mechanisms. A major challenge of AIBs lies in the lack of quantitative information on the transport kinetics, interfacial chemistry, and mechanical properties (for flexible ammonium-ion batteries) at macro-, micro-, or nanoscales. In particular, there have been few studies on the interfacial chemistry such as the formation of SEI films in AIBs.

More experiments and simulations are expected to be intimately combined to understand how the physical and chemical properties of the electrodes and electrolyte affect the electrochemical performance of ammonium-ion batteries. One possible direction is to explore and optimize concentrated electrolytes either in the viscous liquid state or the hydrogel form, which would maximize the potential window and engender more electrode materials that were previously deemed unsuitable for AIBs. By radically altering the primary solvation environments of ions, superconcentration induces a series of extraordinary properties and behaviors, including long-range liquid structures, preferential ion transport, interfacial structures, as well as interphasial chemistries. Researchers can take advantage of the tunability and modularity of the electrolytes to decouple chemical and structural variables to acquire fundamental knowledge of the

https://doi.org/10.1021/acsomega.2c04118
ACS Omega 2022, 7, 33732−33748

underlying charge transport and redox processes in AIBs. Additionally, in situ characterizations via state-of-the-art techniques combined with in-depth theoretical analysis are needed to shed light on the properties of the battery components across multiple length scales and establish the processing−structure−properties relationships for recognizing their roles in the battery performance. On another note, recently, machine learning (ML) has proven success for improving lithium-ion batteries. This method could be translated to AIBs and offer a shortcut to understand the complex interplays among multiple components of AIBs from the macro- to the nanoscale. The utilization of ML may help to address various challenges ranging from mechanistic understanding, to new materials exploitation, to optimization of battery cells. All of the information gained will provide a better scientific understanding of the processes dictating successful fabrication of new ammonium-ion batteries with enhanced performance for potential commercialization.

AUTHOR INFORMATION

Corresponding Author

Ying Wang − *Department of Mechanical & Industrial Engineering, Louisiana State University, Baton Rouge, Louisiana 70803, United States;* orcid.org/0000-0003-4650-9446; Email: ywang@lsu.edu

Author

Shelton F. Kuchena − *Department of Mechanical & Industrial Engineering, Louisiana State University, Baton Rouge, Louisiana 70803, United States*

Complete contact information is available at: https://pubs.acs.org/10.1021/acsomega.2c04118

Notes

The authors declare no competing financial interest.

ACKNOWLEDGMENTS

The authors would like to acknowledge the Economic Development Assistantship (EDA) at Louisiana State University and the Proof of Concept/Prototyping Initiative fund sponsored by Louisiana Board of Regents for financial support of this work.

REFERENCES

(1) Yang, C.; Chen, J.; Ji, X.; Pollard, T. P.; Lu, X.; Sun, C.-J.; Hou, S.; Liu, Q.; Liu, C.; Qing, T.; Wang, Y.; Borodin, O.; Ren, Y.; Xu, K.; Wang, C. Aqueous Li-ion battery enabled by halogen conversion−intercalation chemistry in graphite. *Nature* **2019**, *569*, 245−250.

(2) Huang, Z. D.; Hou, H. S.; Zhang, Y.; Wang, C.; Qiu, X. Q.; Ji, X. B. Layer-tunable phosphorene modulated by the cation insertion rate as a sodium-storage anode. *Adv. Mater.* **2017**, *29* (34), 1702372.

(3) Wang, F.; Fan, X.; Gao, T.; Sun, W.; Ma, Z.; Yang, C.; Han, F.; Xu, K.; Wang, C. High-voltage aqueous magnesium ion batteries. *ACS Central Sci.* **2017**, *3* (10), 1121−1128.

(4) Wang, D.; Wei, C.; Lin, M.; Pan, C.; Chou, H.; Chen, H.; Gong, M.; Wu, Y.; Yuan, C.; Angell, M.; Hsieh, Y.; Chen, Y.; Wen, C.; Chen, C.; Hwang, B.; Chen, C.; Dai, H. Advanced rechargeable aluminium ion battery with a high-quality natural graphite cathode. *Nat. Commun.* **2017**, *8*, 14283.

(5) Jayaprakash, N.; Das, S. K.; Archer, L. A. The rechargeable aluminum-ion battery. *Chem. Commun.* **2011**, *47*, 12610−12612.

(6) Kuchena, S. F.; Wang, Y. Superior polyaniline cathode material with enhanced capacity for ammonium ion storage. *ACS Appl. Energy Mater.* **2020**, *3* (12), 11690−11698.

(7) Xie, M.; Zhao, W.; Mao, Y.; Huang, F. $K_{0.38}(H_2O)_{0.82}MoS_2$ as a universal host for rechargeable aqueous cation (K^+, Na^+, Li^+, NH_4^+, Mg^{2+}, Al^{3+}) batteries. *Dalton Trans.* **2020**, *49*, 3488−3494.

(8) Nightingale, E., Jr. Phenomenological theory of ion solvation − effective radii of hydrated ions. *J. Phys. Chem.* **1959**, *63*, 1381−1387.

(9) Tansel, B. Significance of thermodynamic and physical characteristics on permeation of ions during membrane separation: hydrated radius, hydration free energy and viscous effects. *Sep. Purif. Technol.* **2012**, *86*, 119−126.

(10) Wu, X.; Qi, Y.; Hong, J. J.; Li, Z.; Hernandez, A. S.; Ji, X. Rocking-chair ammonium-ion battery: a highly reversible aqueous energy storage system. *Angew. Chem., Int. Ed.* **2017**, *56*, 13026.

(11) Wang, P.; Zhang, Y. F.; Feng, Z. Y.; Liu, Y. Y.; Meng, C. G. A dual-polymer strategy boosts hydrated vanadium oxide for ammonium-ion storage. *J. Colloid. & Interface Sci.* **2022**, *606*, 1322−1332.

(12) Han, J.; Varzi, A.; Passerini, S. The Emergence of Aqueous Ammonium-Ion Batteries. *Angew. Chem., Int. Ed.* **2022**, *61*, e202115046.

(13) Zhang, R.; Wang, S.; Chou, S.; Jin, H. Research Development on Aqueous Ammonium-Ion Batteries. *Adv. Funct. Mater.* **2022**, *32*, 2112179.

(14) Hurlbutt, K.; Wheeler, S.; Capone, I.; Pasta, M. Prussian blue analogs as battery materials. *Joule* **2018**, *2*, 1950−1960.

(15) Zhang, L.; Chen, L.; Zhou, X.; Liu, Z. Towards high-voltage aqueous metal-ion batteries beyond 1.5 V: the zinc/zinc hexacyanoferrate system. *Adv. Energy Mater.* **2015**, *5*, 1400930.

(16) Jiang, L.; Lu, Y.; Zhao, C.; Liu, L.; Zhang, J.; Zhang, Q.; Shen, X.; Zhao, J.; Yu, X.; Li, H.; Huang, X.; Chen, L.; Hu, Y.-S. Building aqueous K-ion batteries for energy storage. *Nat. Energy* **2019**, *4* (6), 495−503.

(17) Wessells, C. D.; McDowell, M. T.; Peddada, S. V.; Pasta, M.; Huggins, R. A.; Cui, Y. Tunable reaction potentials in open framework nanoparticle battery electrodes for grid-scale energy storage. *ACS Nano* **2012**, *6*, 1688−1694.

(18) Wu, X.; Qi, Y.; Hong, J. J.; Li, Z.; Hernandez, A. S.; Ji, X. Rocking-Chair Ammonium-Ion Battery: A Highly Reversible Aqueous Energy Storage System. *Angew. Chem., Int. Ed.* **2017**, *56*, 13026−13030.

(19) Zhang, X.; Xia, M.; Liu, T.; Peng, N.; Yu, H.; Zheng, R.; Zhang, L.; Shui, M.; Shu, J. Copper hexacyanoferrate as ultra-high rate host for aqueous ammonium ion storage. *Chemical Engineering Journal* **2021**, *421*, 127767.

(20) Zhang, H.; Tian, Y.; Wang, W.; Jian, Z.; Chen, W. Organic Ammonium Ion Battery: A New Strategy for Nonmetallic Ion Energy Storage System. *Angew. Chem.* **2022**, *61*, e202204351.

(21) Wu, X.; Xu, Y.; Jiang, H.; Wei, Z.; Hong, J. J.; Hernandez, A. S.; Du, F.; Ji, X. NH_4^+ topotactic insertion in berlin green: an exceptionally long-cycling cathode in aqueous ammonium-ion batteries. *ACS Applied Energy Materials* **2018**, *1*, 3077−3083.

(22) Xia, M.; Zhang, X.; Yu, H.; Yang, Z.; Chen, S.; Zhang, L.; Shui, M.; Xie, Y.; Shu, J. Hydrogen bond chemistry in Fe_4 [Fe (CN) $_6$] $_3$ host for aqueous NH4+ batteries. *Chemical Engineering Journal* **2021**, *421*, 127759.

(23) Wessells, C. D.; Peddada, S. V.; McDowell, M. T.; Huggins, R. A.; Cui, Y. The effect of insertion species on nanostructured open framework hexacyanoferrate battery electrodes. *J. Electrochem. Soc.* **2011**, *159*, A98.

(24) Li, C.; Yan, W.; Liang, S.; Wang, P.; Wang, J.; Fu, L.; Zhu, Y.; Chen, Y.; Wu, Y.; Huang, W. Achieving a high-performance Prussian blue analogue cathode with an ultra-stable redox reaction for ammonium ion storage. *Nanoscale Horizons* **2019**, *4*, 991−998.

(25) Xing, J.; Fu, X.; Guan, S.; Zhang, Y.; Lei, M.; Peng, Z. Novel KV-Fe Prussian blue analogues nanocubes for high-performance aqueous ammonium ion batteries. *Appl. Surf. Sci.* **2021**, *543*, 148843.

(26) Li, C.; Zhang, D.; Ma, F.; Ma, T.; Wang, J.; Chen, Y.; Zhu, Y.; Fu, L.; Wu, Y.; Huang, W. A High-Rate and Long-Life Aqueous Rechargeable Ammonium Zinc Hybrid Battery. *ChemSusChem* **2019**, *12*, 3732−3736.

(27) Wu, X.; Qi, Y.; Hong, J. J.; Li, Z.; Hernandez, A. S.; Ji, X. Rocking-Chair Ammonium-Ion Battery: A Highly Reversible Aqueous Energy Storage System. *Angew. Chem., Int. Ed.* **2017**, *56*, 13026−13030.
(28) Dong, S.; Shin, W.; Jiang, H.; Wu, X.; Li, Z.; Holoubek, J.; Stickle, W. F.; Key, B.; Liu, C.; Lu, J.; Greaney, P. A.; Zhang, X.; Ji, X.; et al. Ultra-fast NH4+ storage: Strong H bonding between NH4+ and Bi-layered V2O5. *Chem.* **2019**, *5*, 1537−1551.
(29) Song, Y.; Pan, Q.; Lv, H.; Yang, D.; Qin, Z.; Zhang, M.-Y.; Sun, X.; Liu, X.-X. Ammonium-ion storage using electrodeposited manganese oxides. *Angew. Chem., Int. Ed.* **2021**, *60*, 5718−5722.
(30) Xu, W.; Zhang, L.; Zhao, K.; Sun, X.; Wu, Q. Layered ferric vanadate nanosheets as a high-rate NH4+ storage electrode. *Electrochim. Acta* **2020**, *360*, 137008.
(31) Li, H.; Yang, J.; Cheng, J.; He, T.; Wang, B. Flexible aqueous ammonium-ion full cell with high rate capability and long cycle life. *Nano Energy* **2020**, *68*, 104369.
(32) Zhang, Y.; An, Y.; Yin, B.; Jiang, J.; Dong, S.; Dou, H.; Zhang, X. A novel aqueous ammonium dual-ion battery based on organic polymers. *Journal of Materials Chemistry A* **2019**, *7*, 11314−11320.
(33) Deng, J.; Wang, X.; Guo, J.; Liu, P. Effect of the oxidant/monomer ratio and the washing post-treatment on electrochemical properties of conductive polymers. *Ind. Eng. Chem. Res.* **2014**, *53*, 13680−13689.
(34) Holoubek, J. J.; Jiang, H.; Leonard, D.; Qi, Y.; Bustamante, G. C.; Ji, X. Amorphous titanic acid electrode: its electrochemical storage of ammonium in a new water-in-salt electrolyte. *Chem. Commun.* **2018**, *54*, 9805−9808.
(35) Qiu, S.; Xu, Y.; Li, X.; Sandstrom, S. K.; Wu, X.; Ji, X. Reinforced potassium and ammonium storage of the polyimide anode in acetate-based water-in-salt electrolytes. *Electrochem. Commun.* **2021**, *122*, 106880.
(36) Xie, M.; Zhao, W.; Mao, Y.; Huang, F. K 0.38 (H 2 O) 0.82 MoS 2 as a universal host for rechargeable aqueous cation (K+, Na+, Li+, NH 4+, Mg 2+, Al 3+) batteries. *Dalton Transactions* **2020**, *49*, 3488−3494.
(37) Ma, Y.; Sun, T.; Nian, Q.; Zheng, S.; Ma, T.; Wang, Q.; Du, H.; Tao, Z. Alloxazine as anode material for high-performance aqueous ammonium-ion battery. *Nano Research* **2022**, *15*, 2047−2051.
(38) Xia, M.; Zhang, X.; Yu, H.; Yang, Z.; Chen, S.; Zhang, L.; Shui, M.; Xie, Y.; Shu, J. Hydrogen bond chemistry in Fe4 [Fe (CN) 6] 3 host for aqueous NH4+ batteries. *Chemical Engineering Journal* **2021**, *421*, 127759.
(39) Zhang, Y.; An, Y.; Yin, B.; Jiang, J.; Dong, S.; Dou, H.; Zhang, X. A novel aqueous ammonium dual-ion battery based on organic polymers. *Journal of Materials Chemistry A* **2019**, *7*, 11314−11320.
(40) Tian, Z.; Kale, V. S.; Wang, Y.; Kandambeth, S.; Czaban-Jozwiak, J.; Shekhah, O.; Eddaoudi, M.; Alshareef, H. N. High-Capacity NH4+ Charge Storage in Covalent Organic Frameworks. *J. Am. Chem. Soc.* **2021**, *143*, 19178−19186.
(41) Kuchena, S. F.; Wang, Y. V_2O_5 intercalated with polyaniline for improved kinetics in aqueous ammonium-ion batteries. *Electrochim. Acta* **2022**, *425*, 140751.
(42) Ming, J.; Cao, Z.; Wahyudi, W.; Li, M.; Kumar, P.; Wu, Y.; Hwang, J.-Y.; Hedhili, M. N.; Cavallo, L.; Sun, Y.-K.; Li, L.-J.; et al. New insights on graphite anode stability in rechargeable batteries: Li ion coordination structures prevail over solid electrolyte interphases. *ACS Energy Letters* **2018**, *3*, 335−340.
(43) Cheng, H.; Sun, Q.; Li, L.; Zou, Y.; Wang, Y.; Cai, T.; Zhao, F.; Liu, G.; Ma, Z.; Wahyudi, W.; Li, Q.; Ming, J.; et al. Emerging era of electrolyte solvation structure and interfacial model in batteries. *ACS Energy Letters* **2022**, *7*, 490−513.
(44) Tian, Z.; Zou, Y.; Liu, G.; Wang, Y.; Yin, J.; Ming, J.; Alshareef, H. N. Electrolyte Solvation Structure Design for Sodium Ion Batteries. *Advanced Science* **2022**, *9*, 2201207.
(45) Chen, J.; Li, Z.; Sun, N.; Xu, J.; Li, Q.; Yao, X.; Ming, J.; Peng, Z. A Robust Li-Intercalated Interlayer with Strong Electron Withdrawing Ability Enables Durable and High-Rate Li Metal Anode. *ACS Energy Letters* **2022**, *7*, 1594−1603.
(46) Tian, Z.; Kale, V. S.; Wang, Y.; Kandambeth, S.; Czaban-Jozwiak, J.; Shekhah, O.; Eddaoudi, M.; Alshareef, H. N. High-capacity NH4+ charge storage in covalent organic frameworks. *J. Am. Chem. Soc.* **2021**, *143*, 19178−19186.
(47) Wang, P.; Zhang, Y. F.; Feng, Z. Y.; Liu, Y. Y.; Meng, C. G. A dual-polymer strategy boosts hydrated vanadium oxide for ammonium-ion storage. *J. Colloid. & Interface Sci.* **2022**, *606*, 1322−1332.
(48) Borodin, O.; Self, J.; Persson, K. A.; Wang, C.; Xu, K. Uncharted waters: super-concentrated electrolytes. *Joule* **2020**, *4*, 69−100.
(49) Zhang, T.; Tang, Y.; Guo, S.; Cao, X.; Pan, A.; Fang, G.; Zhou, J.; Liang, S. Fundamentals and perspectives in developing zinc-ion battery electrolytes: a comprehensive review. *Energy Environ. Sci.* **2020**, *13*, 4625−4665.
(50) Suo, L.; Borodin, O.; Gao, T.; Olguin, M.; Ho, J.; Fan, X. L.; Luo, C.; Wang, C. S.; Xu, K. Water-in-salt electrolyte enables high-voltage aqueous lithium-ion chemistries. *Science* **2015**, *350*, 938−943.
(51) Chen, Y.; Zhao, J.; Wang, Y. Quasi-solid-state zinc ion rechargeable batteries for subzero temperature applications. *ACS Appl. Energy Mater.* **2020**, *3*, 9058−9065.
(52) Wang, Y.; Chen, Y. H. A flexible zinc-ion battery based on the optimized concentrated hydrogel electrolyte for enhanced performance at subzero temperature. *Electrochim. Acta* **2021**, *395*, 139178.
(53) Holoubek, J. J.; Jiang, H.; Leonard, D.; Qi, Y. T.; Bustamante, G. C.; Ji, X. L. Amorphous titanic acid electrode: its electrochemical storage of ammonium in a new water-in-salt electrolyte. *Chem. Commun.* **2018**, *54*, 9805−9808.
(54) Yan, L.; Qi, Y.; Dong, X. L.; Wang, Y. G.; Xia, Y. Y. Ammonium-ion batteries with a wide operating temperature window from −40 to 80°C. *eScience* **2021**, *1*, 212−218.
(55) Wu, K.; Huang, J. H.; Yi, J.; Liu, X. Y.; Liu, Y. Y.; Wang, Y. G.; Zhang, J. J.; Xia, Y. Y. Recent advances in polymer electrolytes for zinc on batteries: mechanisms, properties, and perspectives. *Adv. Energy Mater.* **2020**, *10*, 1903977.
(56) Chan, C. Y.; Wang, Z.; Jia, H.; Ng, P. F.; Chow, L.; Fei, B. Recent advances of hydrogel electrolytes in flexible energy storage devices. *J. Mater. Chem., A* **2021**, *9*, 2043−2069.
(57) Becker, A.; Katzen, F.; Pühler, A.; Ielpi, L. Xanthan gum biosynthesis and application: a biochemical /genetic perspective. *Appl. Microbiol. Biotechnol.* **1998**, *50*, 145.
(58) Katzbauer, B. Properties and applications of xanthan gum. *Polym. Degrad. Stab.* **1998**, *59*, 81−84.
(59) Morelle, X. P.; Illeperuma, W. R.; Tian, K.; Bai, R. B.; Suo, Z. G.; Vlassak, J. J. Highly stretchable and tough hydrogels below water freezing temperature. *Adv. Mater.* **2018**, *30*, 1801541.
(60) Liang, G.; Wang, Y.; Huang, Z.; Mo, F.; Li, X.; Yang, Q.; Wang, D.; Li, H.; Chen, S.; Zhi, C. Initiating hexagonal MoO3 for superb-stable and fast NH4+ storage based on hydrogen bond chemistry. *Adv. Mater.* **2020**, *32*, 1907802.
(61) Farai Kuchena, S.; Wang, Y. A full flexible NH_4^+ ion battery based on the concentrated hydrogel electrolyte for enhanced performance. *Chem.—Eur. J.* **2021**, *27*, 15450−15459.
(62) Zeng, W.; Shu, L.; Li, Q.; Chen, S.; Wang, F.; Tao, X. Fiber-based wearable electronics: a review of materials, fabrication, devices, and applications. *Adv. Mater.* **2014**, *26*, 5310−5336.
(63) Kim, J.; Kumar, R.; Bandodkar, A.; Wang, J. Advanced materials for printed wearable electrochemical devices: a review. *Adv. Electro. Mater.* **2017**, *3*, 1600260.
(64) Jia, W.; Wang, X.; Imani, S.; Bandodkar, A. J.; Ramirez, J.; Mercier, P. P.; Wang, J. Wearable textile biofuel cells for powering electronics. *Journal of Materials Chemistry A* **2014**, *2*, 18184−18189.
(65) Stoppa, M.; Chiolerio, A. Wearable electronics and smart textiles: A critical review. *sensors* **2014**, *14*, 11957−11992.
(66) Liu, Z.; Mo, F.; Li, H.; Zhu, M.; Wang, Z.; Liang, G.; Zhi, C. In situ growth of a high-Performance All-solid-state electrode for flexible supercapacitors based on a PANI/CNT/EVA composite. *Small Methods* **2018**, *2*, 1800124.

https://doi.org/10.1021/acsomega.2c04118
ACS Omega 2022, 7, 33732−33748

(67) Zhang, Y.; An, Y.; Yin, B.; Jiang, J.; Dong, S.; Dou, H.; Zhang, X. A novel aqueous ammonium dual-ion battery based on organic polymers. *Journal of Materials Chemistry A* **2019**, *7*, 11314−11320.
(68) Li, C.; Zhang, D.; Ma, F.; Ma, T.; Wang, J.; Chen, Y.; Zhu, Y.; Fu, L.; Wu, Y.; Huang, W. A High-Rate and Long-Life Aqueous Rechargeable Ammonium Zinc Hybrid Battery. *ChemSusChem* **2019**, *12*, 3732−3736.
(69) Miller, J. R.; Simon, P. Electrochemical capacitors for energy management. *science* **2008**, *321*, 651−652.
(70) Gonzalez, A.; Goikolea, E.; Barrena, J. A.; Mysyk, R. Review on supercapacitors: Technologies and materials. *Renewable and sustainable energy reviews* **2016**, *58*, 1189−1206.
(71) Wang, P.; Zhang, Y.; Jiang, H.; Dong, X.; Meng, C. Ammonium vanadium oxide framework with stable NH4+ aqueous storage for flexible quasi-solid-state supercapacitor. *Chemical Engineering Journal* **2022**, *427*, 131548.
(72) Wang, P.; Zhang, Y.; Feng, Z.; Liu, Y.; Meng, C. A dual-polymer strategy boosts hydrated vanadium oxide for ammonium-ion storage. *J. Colloid Interface Sci.* **2022**, *606*, 1322−1332.
(73) Chen, X.; Wang, P.; Feng, Z.; Meng, C.; Zhang, Y. Conductive polymer intercalated vanadium oxide on carbon cloth for fast ammonium-ion storage in supercapacitor applications. *Chemical Engineering Journal* **2022**, *445*, 136747.
(74) Lakshmi, K.C. S.; Ji, X.; Chen, T.-Y.; Vedhanarayanan, B.; Lin, T.-W. Pseudocapacitive and battery-type organic polymer electrodes for a 1.9 V hybrid supercapacitor with a record concentration of ammonium acetate. *J. Power Sources* **2021**, *511*, 230434.

https://doi.org/10.1021/acsomega.2c04118
ACS Omega 2022, 7, 33732−33748